

RESEARCH

Open Access



Distinct gut microbiome characteristics and dynamics in patients with Parkinson's disease based on the presence of premotor rapid-eye movement sleep behavior disorders

Jae-Yun Lee^{1†}, Sungyang Jo^{2†}, Jihyun Lee², Moongwan Choi², Kijeong Kim², Sangjin Lee², Hyun Sik Kim¹, Jin-Woo Bae^{1*} and Sun Ju Chung^{2*}

Abstract

Background Alpha-synuclein aggregation, a hallmark of Parkinson's disease (PD), is hypothesized to often begin in the enteric or peripheral nervous system in "body-first" PD and progresses through the vagus nerve to the brain, therefore REM sleep behavior disorder (RBD) precedes the PD diagnosis. In contrast, "brain-first" PD begins in the central nervous system. Evidence that gut microbiome imbalances observed in PD and idiopathic RBD exhibit similar trends supports body-first and brain-first hypothesis and highlights the role of microbiota in PD pathogenesis. However, further investigation is needed to understand distinct microbiome changes in body-first versus brain-first PD over the disease progression.

Results Our investigation involved 104 patients with PD and 85 of their spouses as healthy controls (HC), with 57 patients (54.8%) categorized as PD-RBD(+) and 47 patients (45.2%) as PD-RBD(-) based on RBD presence before the PD diagnosis. We evaluated the microbiome differences between these groups over the disease progression through taxonomic and functional differential abundance analyses and carbohydrate-active enzyme (CAZyme) profiles based on metagenome-assembled genomes. The PD-RBD(+) gut microbiome showed a relatively stable microbiome composition irrespective of disease stage. In contrast, PD-RBD(-) microbiome exhibited a relatively dynamic microbiome change as the disease progressed. In early-stage PD-RBD(+), *Escherichia* and *Akkermansia*, associated with pathogenic biofilm formation and host mucin degradation, respectively, were enriched, which was supported by functional analysis. We discovered that genes of the UDP-GlcNAc synthesis/recycling pathway negatively correlated with biofilm formation; this finding was further validated in a separate cohort. Furthermore, fiber intake-associated taxa were decreased in early-stage PD-RBD(+) and the biased mucin-degrading capacity of CAZyme compared to fiber degradation.

Conclusion We determined that the gut microbiome dynamics in patients with PD according to the disease progression depend on the presence of premotor RBD. Notably, early-stage PD-RBD(+) demonstrated distinct gut microbial

[†]Jae-Yun Lee and Sungyang Jo contributed equally to this work.

*Correspondence:

Jin-Woo Bae

baejw@khu.ac.kr

Sun Ju Chung

sjchung@amc.seoul.kr



characteristics, potentially contributing to exacerbation of PD pathophysiology. This outcome may contribute to the development of new therapeutic strategies targeting the gut microbiome in PD.

Keywords Parkinson's disease, Microbiome, Rapid eye movement sleep behavior disorders, Biofilm, Carbohydrate-active enzymes

Background

Alpha-synuclein aggregation, a pathologic marker of Parkinson's disease (PD), is found in the extranigral area even in early-stage PD, especially in the dorsal motor nucleus of the vagus nerve and enteric nervous system. Braak et al. hypothesized that alpha-synuclein may propagate from the peripheral nervous system to the central nervous system [1, 2], and phosphorylated alpha-synuclein positivity was identified in gastrointestinal nerve fibers years prior to the PD diagnosis [3]. Moreover, animal studies have demonstrated that injection of preformed alpha-synuclein fibrils into the mouse duodenum results in the propagation of alpha-synuclein in the brain via the vagus nerve, suggesting a potential connection between the gut and alpha-synuclein aggregation in PD [4].

However, not all PD patients exhibit pathology that begins in the enteric nervous system. Some PD autopsy cases revealed no pathologic alpha-synuclein inclusions in the dorsal motor nucleus of the vagus nerve in the pons, whereas other cases featuring limbic-predominant alpha-synuclein inclusions exhibited minimal brainstem involvement [5]. Based on these findings, the concepts of “body-first” PD, where pathology originates in the enteric or peripheral nervous system, and “brain-first” PD, where pathology begins in the central nervous system descending to the peripheral nervous system emerged. A key distinguishing feature of the body-first PD is the presence of idiopathic REM sleep behavior disorder (RBD) several years prior to the PD diagnosis, indicating pathology propagation from the subcoeruleus complex in the pons to the substantia nigra. Moreover, 35–60% of patients diagnosed with PD exhibited RBD prior to their PD diagnosis (premotor RBD) [6], and these patients demonstrated significantly higher enteric alpha-synuclein histopathology than patients with PD without premotor RBD [7], and slower colon transit time [5].

The gut microbiome of PD patients was imbalanced and had lower diversity compared to healthy controls (HC) [8]. A meta-analysis uncovered a decrease in short-chain fatty acid producers, such as *Faecalibacterium* and *Roseburia*, and an increase in the mucin-degrading genus *Akkermansia* in PD [8], which were associated with accelerated disease progression [9]. Additionally, animal experiments have demonstrated that curli protein produced by *Escherichia coli* cross-seeds with alpha-synuclein, thereby promoting alpha-synuclein aggregation

[10, 11]. A recent study also showed that bacterial curli combined with a fiber-deprived diet reduce gut barrier integrity, increase the intestinal and brain alpha-synuclein, and alter the microbiome, leading to motor performance in the animal model [12]. We can hypothesize that body-first PD patients might be significantly influenced by the gut microbiome; potentially, this change could contribute to the pathogenesis of PD. This is supported by previous studies showing that altered gut microbiota composition in idiopathic RBD exhibits trends similar to those observed in PD [13–15]. Furthermore, in brain-first PD, RBD may manifest after PD diagnosis due to pathology extending from the substantia nigra to the pons, and the microbiome differences between these two groups may be attenuated as the disease progresses.

However, there are still some uncertainties: it remains unclear whether microbial changes will differ between body-first PD and brain-first PD. Considering the bidirectional gut-brain communication, neurodegeneration can influence gut function and modify the microbiota, as in brain-first PD. Additionally, PD pathology develops over time in both brain-first and body-first PD; it is reasonable to predict that the gut microbiome will undergo changes in both types as the disease progresses. The aim of this study is to investigate how the presence of RBD affects gut microbiome composition and function over the disease progression. Additionally, we conducted a characterization of gut microbiome composition and function in the early stages of the disease.

Materials and methods

Study population

In this prospective case–control study, we enrolled patients with PD and their spouses as HCs at Asan Medical Center from 2019 to 2024. The patients fulfilled the UK Brain Bank criteria for PD [16]. The research work design is elaborated in a prior study [17], and we amassed additional PD patients without premotor RBD to the prior cohort in 2024 ($n=19$), since the preceding cohort included fewer PD patients without premotor RBD than PD patients with RBD. We gathered information regarding age at study enrollment, sex, body mass index, disease duration, PD medication, and disease severity as Hoehn and Yahr stage and United Parkinson's Disease Rating Scale (UPDRS). Diet was evaluated utilizing a semi-quantitative food frequency questionnaire [18]. Irritable bowel

syndrome (IBS) and constipation were assessed using the ROME III diagnostic criteria [19]. As a routine practice, we interviewed the patients with PD regarding the presence of RBD at the time of PD diagnosis using the RBD Single-Question Screen (RBD1Q) [20]. Subsequently, we could use electronic medical records to examine the presence of premotor RBD based on RBD1Q. We categorized the patients into PD with premotor RBD (PD-RBD[+]) and patients with PD without premotor RBD (PD-RBD[-]) groups.

Stool sample collection and sequencing

Stool samples of patients with PD without premotor RBD were collected using stool sampling kits (CJ Bioscience Inc., Seoul, Korea) and stored at -80°C until use. DNA was extracted using a DNeasy PowerSoil Pro Kit (QIAGEN, Hilden, Germany) that adhered to the manufacturer's instructions. The extracted DNA was quantified utilizing the Quant-IT PicoGreen (Invitrogen). For shotgun metagenome sequencing, sequencing libraries were prepared by TruSeq Nano DNA High Throughput Library Prep Kit (Illumina) according to the manufacturer's instructions. Sequencing was conducted utilizing the Illumina NovaSeq X platform (2×150 bp). For the 16S rRNA gene amplicon sequencing, the extracted DNA was amplified using PCR with 16S rRNA gene V3–V4 hypervariable region primers: forward, 341F (5'-TCG TCG GCA GCG TCA GAT GTG TAT AAG AGA CAG CCT ACG GGN GGC WGC AG-3'); reverse, 805R (5'-GTC TCG TGG GCT CGG AGA TGT GTA TAA GAG ACA GGA CTA CHV GGG TAT CTA ATC C-3'). The sequencing library was prepared with the Nextera XT Index (Illumina) and then sequenced using the Illumina MiSeq platform (2×300 bp).

16S rRNA gene amplicon sequencing data analysis

V3–V4 PCR primer sequences in raw reads were trimmed utilizing the Cutadapt (v4.0) [21] with the flags “–discard-untrimmed” and “–match-read-wildcards.” Subsequently, trimmed reads were imported into Qiime2 (v2022.11) [22] and underwent DADA2 (v1.22) [23] denoising. Taxonomic classification of amplicon sequence variants (ASVs) was performed using the Naïve Bayes classifier via scikit-learn (v0.24.1) [24] in a q2-feature-classifier [25], trained on the SILVA 138 SSURef NR99 database [26, 27]. ASVs not classified into the domain Bacteria were excluded from downstream analysis. A phylogenetic tree was established using SATé-enabled phylogenetic placement (SEPP) [28] through the q2-fragment-insertion plugin [29], based on the SILVA 128 SEPP reference database.

Taxonomic and functional profiling of shotgun metagenome sequencing data

The raw metagenomic reads were processed using KneadData (v0.12.0) (<http://huttenhower.sph.harvard.edu/kneaddata>) [30]. Quality filtering and adapter trimming were employed using Trimmomatic (v0.39) [31] and host-derived reads were removed using Bowtie2 (v2.5.1) [32] with the GRCh38 human genome. Taxonomic compositions were profiled via MetaPhlan4 (v4.0.1) [33] employing the mpa_vJan21_CHOCOPHlanSGB database. Functional composition was profiled using HUMAnN3 (v3.6) [34] based on the UniRef90 database [35] which was then regrouped into the Kyoto Encyclopedia of Genes and Genomes (KEGG) orthology (KO) profiles [36] using the “humann_regroup_table” script. The annotation of KOs to the KEGG pathway was conducted using the KEGG Mapper [37] and R package Pathview (v1.38.0) [38]. KEGG enrichment analysis for differentially abundant KOs was performed using the R package MicrobiomeProfiler (v1.4.0) [39].

For large-scale cohort data analysis, sequencing data from Wallen et al. [40] were downloaded from NCBI SRA (BioProject accession no. PRJNA834801) and subsequently analyzed as described above. Data pertaining to current antibiotic use or gastrointestinal disease were excluded from the downstream analysis. Consequently, data from eligible individuals (157 controls and 294 PD) were utilized for the analysis.

Beta diversity analysis

Taxonomic and functional composition tables, except for MetaPhlan4 outputs which formed the relative abundance table, were rarefied to minimum sample depths prior to diversity analysis. UniFrac distances [41] were calculated using the R package rbiom (v1.0.3). The resulting high-dimensional matrices were analyzed to principal coordinate analysis (PCoA) for dimensionality reduction using the stats (v4.2.1). The PCoA were visualized using ggplot2 (v3.4.2). Next, the statistical significances were identified using permutational multivariate analysis of variance (PERMANOVA) through vegan (v2.6.4). For pairwise PERMANOVA testing, *p* values were adjusted using Hommel's method, unless indicated otherwise. Throughout the manuscript, adjusted *p*-values are referred to as *q* values.

Differential abundance analysis

We utilized the currently developed differential abundance (DA) analysis methods, MaAsLin2 [42] with compound Poisson linear models (v1.12.0) and ANCOM-BC [43] (v2.0.3; for function composition data). In the taxonomy and CAZyme DA analysis, any features present

in less than 10% of all samples were filtered out. In the function DA analysis, features present in less than 15% were filtered out. For multiple testing, p values were corrected using the Benjamini–Hochberg method to control false discovery rates. The q value < 0.1 was considered significant.

Enterosignature decomposition

The enterosignature (ES) profile was determined as described by Frioux et al. [44]. We utilized the pre-trained ES model provided by the authors (<https://gitlab.inria.fr/cfrioux/enterosignature-paper/>) and adjusted the taxonomic features between our feature table and pre-trained ES model. Subsequently, the ES composition was profiled using the “reapply_nmf.py” script and visualized using the R package ggplot2 (v3.4.2).

Metagenome-assembled genomes reconstruction

The raw metagenomic reads were processed using BBTools (v39.01, <https://jgi.doe.gov/data-and-tools/software-tools/bbtools/>). Host-derived contaminants were mapped to the GRCh38 human genome using Bowtie2. Next, mapped reads were filtered out using SAMtools [45] (v1.16.1). Each sample's processed reads were individually assembled using SPAdes [46] (v3.15.5) with a “-meta” mode. Contigs of length ≥ 1 kb were utilized for the downstream metagenome-assembled genomes (MAG) analysis. The reads were mapped back to the contigs from the corresponding metagenome as well as to the contigs from each of the 39 different metagenomes using Bowtie2 to generate the contig depth information. Contigs from each metagenome were individually binned using MetaBAT2 [47] (v2.15), MaxBin2 [48] (v2.2.7), and CONCOCT [49] (v1.1.0). Output MAGs were further refined using the DAS Tool [50] (v1.1.6). The quality of the bins was assessed using CheckM [51] (v1.2.2) with lineage-specific workflows and bins with completeness $< 50\%$ or contamination $> 5\%$ were excluded from the downstream analysis. Taxonomy was annotated utilizing GTDB-Tk [52] (v2.2.6). Open reading frames of the MAGs were predicted by using Prodigal [53] (v2.6.3) and annotated by using Prokka [54] (v1.14.6) with default, PGAP, and Pfam databases. KEGG orthology (KO) annotation was conducted using KofamScan [55] (v1.3.0).

CsgA sequence analysis with MAGs

Curli major subunit CsgA sequences of the MAGs were retrieved from the annotation results. Reference CsgA sequences of *E. coli* and *Citrobacter youngae* were downloaded from UniProt with the accession numbers P28307 and A0A9Q7ZLGO, respectively. A multiple sequence alignment was conducted utilizing Clustal Omega [56] (v1.2.4). The phylogenetic tree of the sequences was

constructed using IQ-TREE [57] (v1.6.12) with default parameters. The result of multiple sequence alignment was imported into R using Biostrings (v2.72.1) and then visualized using ggseqlogo (v0.2) and ggplot2 (v3.4.2).

CAZyme prediction using MAGs

The CAZymes of each bin and corresponding substrate were annotated using dbCAN3 [58]. Read coverages were determined using featureCounts [59] (v2.0.4) and then normalized by gene length. Mucin- and fiber-targeting CAZymes were identified based on previous studies (Additional file 2: Table S1).

Correlation analyses

Spearman's rank and Pearson correlation coefficients were calculated using the R package rstatix (v0.7.2). For taxonomic and functional feature tables, the centered-log ratio (CLR) method was applied using the R package microbiome (v1.20.0) prior to conducting correlation analyses. Features observed in less than 10% of the samples were excluded from the analyses. Correlation results with q value < 0.05 and an absolute rho coefficient ($|\rho| \geq 0.3$) were further utilized for visualization in Cytoscape (v3.10.0) [60]. For visualization of the results from Wallen et al. [40], the R package rstatix was used. P values were adjusted using Benjamini–Hochberg correction to control the false discovery rate.

Other statistical analysis and visualization

Fisher's exact test, Pearson's chi-squared test, Wilcoxon rank-sum test, and Kruskal–Wallis H test were performed using R package stats. For additional visualizations, R packages ggplot2 (v3.4.2), patchwork (v1.1.2.9000), ggsignif (v0.6.4), ggalluvial (v0.12.5), ggrepel (v0.9.3), and ggpubr (v0.6.0) were utilized. Considering the significant difference in age across groups (Table 1), especially in the late stage (Supplementary table S6), age was adjusted as a covariate in the analyses when using the entire sample or late-stage data. Linear regression analysis was conducted using *lm* function of R package stat (v4.3.1). Power analysis was conducted using R package micropower (v0.4) [61].

Results

Baseline demographics

Of the 112 patients with PD and 85 HC, we excluded 8 patients with PD due to a lack of information on RBD prior to the PD diagnosis. Among 104 PD patients, 57 PD patients had RBD before the PD diagnosis (PD-RBD[+]), while 47 PD patients did not have RBD prior to the PD diagnosis (PD-RBD[-]). The PD-RBD(-) group was younger than both the PD-RBD(+) and HC groups (p value = 0.028), and there were no significant differences

Table 1 Baseline demographics of patients with Parkinson's disease (PD) and the healthy controls (HC)

	PD-RBD(+) (n = 57)	PD-RBD(-) (n = 47)	HC (n = 85)	P value
Age, mean (SD)	66.1 ± 7.1	61.9 ± 8.8	64.6 ± 8.0	0.03
Male, n (%)	36 (63.2%)	19 (40.4%)	40 (47.1%)	0.05
BMI (kg/m ²), median (IQR)	24.3 (22.3–26.7)	24.5 (22.2–26.6)	23.9 (21.5–25.5)	0.26
Education (years), median (IQR)	12.0 (9.0–16.0)	12.0 (12.0–16.0)	12.0 (12.0–16.0)	0.33
IBS, n (%)	1 (1.8%)	1 (2.1%)	3 (3.5%)	0.79
Constipation, n (%)	29 (50.9%)	18 (38.3%)	11 (12.9%)	< 0.001
Disease duration (years), median (IQR)	2.0 (0.0–7.0)	2.0 (1.0–4.5)	–	0.94
Hoehn & Yarh stage, median (IQR)	2.0 (2.0–3.0)	2.0 (2.0–3.0)	–	0.59
UPDRS Part 3 score, mean (SD)	33.0 ± 13.0	29.9 ± 9.9	–	0.28
UPDRS total score, mean (SD)	48.0 ± 19.5	43.7 ± 15.3	–	0.33
Use of levodopa, n (%)	45 (80.4%)	40 (85.1%)	–	0.30
Use of dopamine agonist, n (%)	18 (32.1%)	23 (48.9%)	–	0.08
Use of COMT inhibitor, n (%)	2 (3.6%)	7 (14.9%)	–	0.09
Use of MAO inhibitor, n (%)	17 (30.4%)	8 (17.0%)	–	0.18
Use of amantadine, n (%)	12 (21.4%)	9 (19.1%)	–	0.97
Levodopa equivalent daily dose	450.0 (225.0–711.2)	450.0 (300.0–730.0)	–	0.96

BMI body mass index, COMT catechol-O-methyltransferase, IBS irritable bowel syndrome, UPDRS unified Parkinson's disease rating scale, MAO monoamine oxidase, IQR interquartile range, RBD rapid eye movement sleep behavior disorder

in sex, BMI, or the presence of IBS (Table 1). Constipation was significantly higher in the PD groups compared to the HC group (p value < 0.001). There were no significant differences in medication use (for PD, constipation, insomnia, and depression), levodopa equivalent daily dose (LEDD; value representing intensity of dopaminergic treatment), and dietary intake between the PD-RBD(+) and PD-RBD(-) groups (Table 1 and Supplementary Table S1). Stool samples were collected and analyzed by 16S rRNA gene amplicon sequencing and/or shotgun metagenome sequencing: total of 185 samples—including 55 patients in PD-RBD(+), 46 patients in PD-RBD(-) and 84 HC—were used for 16S rRNA gene amplicon sequencing, and 166 stool samples—51 patients in PD-RBD(+), 42 patients in PD-RBD(-), and 73 HC—were used for shotgun metagenome sequencing.

Differences in the gut microbiome between PD-RBD(+) and PD-RBD(-) were attenuated as the disease progressed

At the early-stage of disease (< 2 years after PD diagnosis), gut microbial compositions of PD-RBD(+) were significantly different from those of PD-RBD(-) (shotgun metagenome sequencing [shotgun]: $R^2=0.05$, q value = 0.045; 16S rRNA gene amplicon sequencing [16S]: $R^2=0.043$, q value = 0.009) and HC (shotgun: $R^2=0.038$, q value = 0.003; 16S: $R^2=0.021$, q value = 0.006) (Fig. 1A, B) in beta-diversity analysis. On the other hand, early-stage PD-RBD(-) showed no significant compositional difference compared with HC (shotgun: $R^2=0.021$, q value = 0.078; 16S: $R^2=0.013$, q value = 0.15). In the

late-stage PD-RBD(+), consistent with early-stage findings, the gut microbiome still exhibited a significant deviation from the HC (shotgun: $R^2=0.025$, q value = 0.028; 16S: $R^2=0.013$, q value = 0.042 with age as a covariate) (Fig. 1C–F). However, unlike in the early stage, the gut microbiomes of PD-RBD(+) and PD-RBD(-) in the late stage became closer to each other (shotgun: $R^2=0.030$, q -value = 0.075; 16S: $R^2=0.021$, q value = 0.198 with age as a covariate). Moreover, gut microbiome of late-stage PD-RBD(-) deviated from HC (shotgun: $R^2=0.023$, q value = 0.028; 16S: $R^2=0.015$, q value = 0.036 with age as a covariate), in contrast to the similar pattern observed in the early stage. The distinct gut microbiome composition between early-stage PD-RBD(+) and PD-RBD(-), as well as their relatively similar composition in the late stage, remained consistent even after adjusting for the use of levodopa or the LEDD as a covariate (Additional file 1: Supplementary Table S2). To assess the statistical power of PERMANOVA, we conducted the power estimation method using the unbiased effect size estimator (ω^2) [61]. The analysis revealed that a sample size of 20 per group provided 90% power to detect a ω^2 of 0.012 and 0.019 for 16S and shotgun data, respectively. In PERMANOVA test involving smaller sample sizes in both groups—early-stage PD-RBD(+) and PD-RBD(-) (Fig. 1 A and B)—the corresponding ω^2 values were 0.019 and 0.027 for 16S and shotgun data, respectively, allowing for 90% power.

In the correlation analysis, longer disease duration of PD-RBD(-) was positively correlated with deviations in gut microbiome composition from that in the

HC (shotgun: Pearson's $r=0.14$, p value= $3.7e-15$; 16S: $r=0.19$, p value $<2.2e-16$) (Fig. 1G, H) and the early-stage disease within the same group (shotgun: $r=0.21$, p value= $9e-06$; 16S: $r=0.24$, p value= $1.6e-08$) (Fig. 1I, J). The same analysis on PD-RBD(+) showed a non-significant result or profoundly smaller correlation coefficients than those in PD-RBD(-) (Distances to HC—shotgun: $r= -3.7e-3$, p value= 0.82 ; 16S: $r=0.15$, p value $<2.2e-16$ —and distances to early-stage disease—shotgun: $r=0.031$, p value= 0.44 ; 16S: $r=0.13$, $p=2.4e-4$) (Fig. 1G–J). Even when accounting for age as a covariate in a linear regression model, PD-RBD(+) exhibited a relatively stable microbiome (its distance from HC or from its early stage did not increase with disease duration), whereas PD-RBD(-) showed a relatively dynamic microbiome (showing an increasing distance from HC or from its early stage as disease duration progressed) (Additional file 1: Supplementary Tables S3 and S4). The interaction between disease duration and PD-RBD(-) also showed a significant positive association (Additional file 1: Supplementary Tables S3 and S4).

Therefore, we focused on investigating the gut microbiome of patients with early-stage PD (<2 years after PD diagnosis) in further studies when the microbiome differences between PD-RBD(+) and PD-RBD(-) were prominent. In early-stage PD, age, sex, BMI, presence of IBS and constipation, LEDD, and use of medications (for PD, constipation, insomnia, and depression) were not significantly different between PD-RBD(+) and PD-RBD(-) groups (Additional file 1: Supplementary Table S5). The characteristics of late-stage PD (≥ 2 years after PD diagnosis) are detailed in Supplementary Table S6. Furthermore, apart from levodopa, the usage rates of other medications were generally low, particularly in the early stage (Additional file 1: Supplementary Table S5). The analysis of individual items from the ROME III criteria revealed that early-stage PD-RBD(+) patients had significantly higher rates of straining during defecation

compared to early-stage PD-RBD(-) patients, and they also tended to have a higher proportion of lumpy or hard stools (Additional file 1: Supplementary Table S5). However, these trends were not observed in the late-stage PD-RBD(+) group (Additional file 1: Supplementary Table S6).

Distinct taxonomic features in the gut microbiome of early-stage PD-RBD(+)

To identify the differential taxa among PD-RBD(+), PD-RBD(-), and HC, we employed DA analysis using both shotgun metagenomics and 16S rRNA gene amplicon data (Additional file 3). In PD-RBD(+), an increased abundance of genera *Escherichia* (when compared to PD-RBD(-)), *Desulfovibrio*, *Barnesiella*, *Eisenbergiella* (when compared to HC), *Akkermansia* and *Hungatella* (when compared to both PD-RBD(-) and HC) was found on shotgun data (Fig. 2A and B). Notably, these genera are abundantly reported in relation to the PD gut microbiome [14, 17, 40, 62–67]. *Escherichia coli* has recently garnered attention due to its potential link with PD pathogenesis, especially because of its ability to generate curli amyloid fibrils [10–12, 68–70]. *Akkermansia* and *Barnesiella* specialize in mucin degradation [71], thereby diminishing the intestinal mucus layer. Additionally, previous studies demonstrated an increase in *Akkermansia* and *Desulfovibrio* in idiopathic RBD patients and PD-RBD(+) patients [13]. *Eisenbergiella* and *Hungatella* have been identified as enriched in patients with PD [40, 62, 72, 73] and multiple sclerosis [74]; moreover, *Eisenbergiella* is also increased in PD-RBD(+). However, the specific mechanisms linking these bacteria to disease pathology remain unclear and necessitate further investigations.

Prevotella, *Faecalibacterium*, and *Agathobaculum* were lower than HC in PD-RBD(+) on shotgun data (Fig. 2A and C). *Prevotella* and *Faecalibacterium* demonstrated a positive association with fiber intake [75–77], and

(See figure on next page.)

Fig. 1 Different gut microbiome alteration patterns in PD-RBD(+) and PD-RBD(-) depending on disease progression. **A, B** Principal coordinate analysis (PCoA) plots based on the unweighted UniFrac distance matrix using **(A)** shotgun metagenome and **(B)** 16S amplicon sequencing data from patients with early-stage PD and HC. Overall and pairwise permutational analysis of variance (PERMANOVA) were utilized to ascertain the significance of gut microbiome differences across groups. Bonferroni correction was implemented to adjust the p-value in pairwise PERMANOVA. Large circles represent the centroids for each group. The ellipses represent the 95% confidence interval. **C, D** The unweighted UniFrac distance-based PCoA illustrates gut microbiome variations across the disease stages: early (less than 2 years after PD diagnosis) and late (greater than or equal to two years after PD diagnosis). **E, F** Results of pairwise PERMANOVA analyses encompassing early- and late-stage of PD-RBD(+) and PD-RBD(-). Age was used as a covariate due to the age differences observed in late-stage samples, as shown in Supplementary table S6. **G, H** Unweighted UniFrac distances from PD-RBD(+) (blue) and PD-RBD(-) (red) to HC across the disease duration, employing **(G)** shotgun metagenome and **(H)** 16S rRNA gene amplicon data, respectively. **I, J** Unweighted UniFrac distances of PD-RBD(+) (blue) and PD-RBD(-) (red) from the late stages to their respective early stages, using **(I)** shotgun metagenome and **(J)** 16S rRNA gene amplicon data, respectively. *** $p < 0.001$ for PERMANOVA. * $q < 0.05$; ** $q < 0.01$ for pairwise PERMANOVA. ns not significant, r Pearson correlation coefficient, PD Parkinson's disease, RBD rapid eye movement sleep behavior disorder, HC healthy control

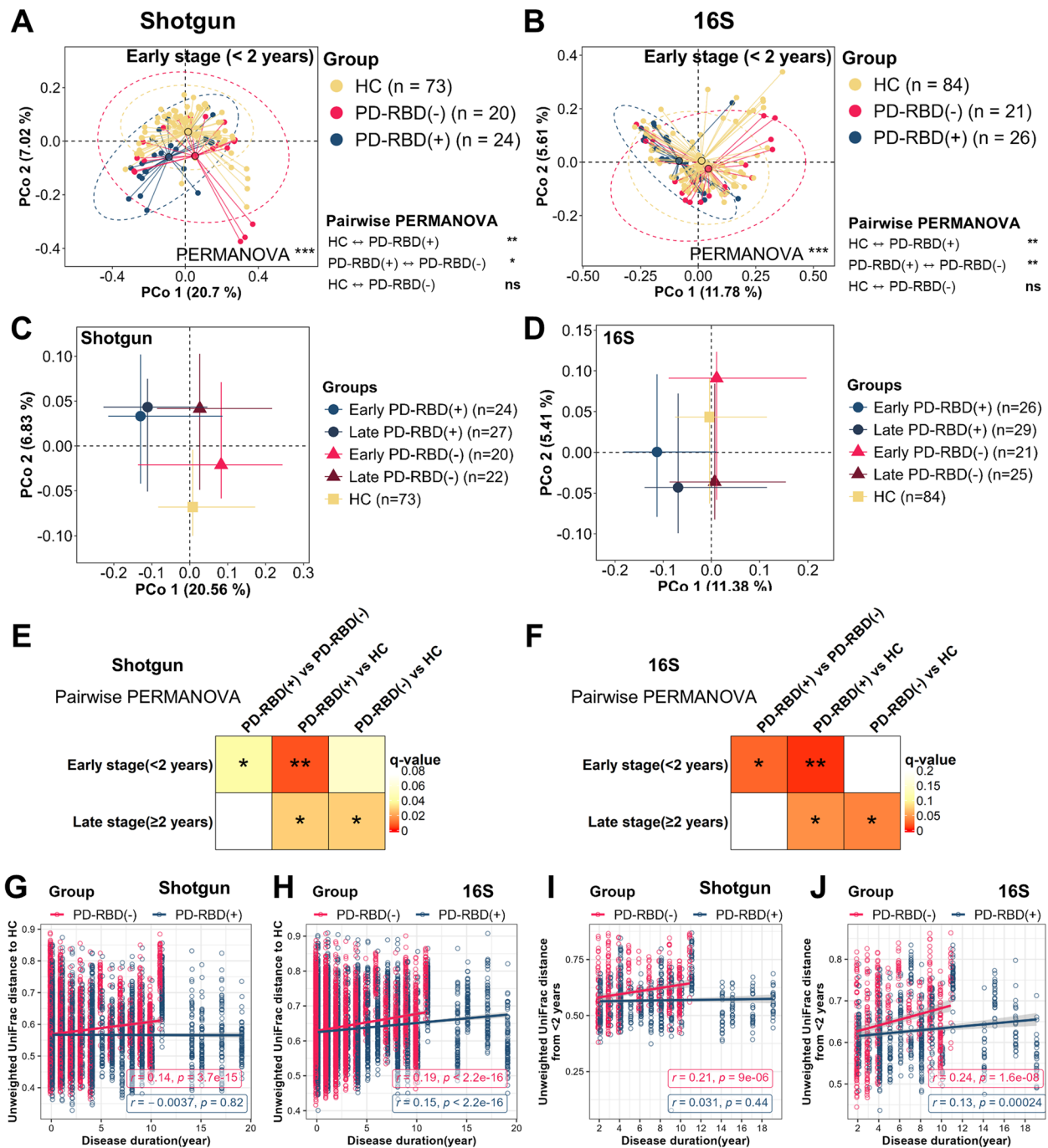


Fig. 1 (See legend on previous page.)

Agathobaculum was reported to exert neuroprotective effects in the intrastriatal 6-hydroxydopamine lesion-induced PD mouse model via the AKT/GSK3 β signaling pathway [78]. The overall taxonomic characteristics of PD-RBD(+) displayed comparable trends of enrichment or depletion when compared to both HC and PD-RBD(-) samples (Spearman's $\rho = 0.36, p \text{ value} = 2.5e-5$) (Fig. 2E).

In PD-RBD(-), genera *Coprobacter*, *Erysipelatoclostridium* (currently renamed to *Thomasclavelia*), *Leuconostoc* (when compared to HC), and *Citrobacter* (when compared to PD-RBD(+)) were enriched (Fig. 2 A and D). *Coprobacter* and *Erysipelatoclostridium* have been reported to increase in patients with Alzheimer's disease [79], neurosyphilis [80], and autism [81] as well as

PD [82], but not in idiopathic RBD or PD-RBD(+) in the previous studies [62]. Although the role of *Citrobacter* in PD is not yet known, *Citrobacter* is also known for producing curli amyloid fibrils; however, its curli exhibits a significantly lower propensity to aggregation with alpha-synuclein compared to that of *Escherichia* [70]. The 16S data at the genus or higher taxonomic levels (Fig. S1) and shotgun data at the species level (Fig. S2) mirrored the results obtained from the shotgun data at the genus level (Fig. 2).

In summary, our data highlights a significant discrepancy in a gut microbiome of PD-RBD(+) compared to that of HC as PD-RBD(-), characterized by the increase of curli-producing *Escherichia* and mucin-degrading bacteria, and depletion of bacteria associated with fiber intake. In contrast, PD-RBD(-) demonstrated distinct gut microbiome different from PD-RBD(+) or HC, and some of which were associated with other neurological disorders, but not idiopathic RBD.

Dysbiotic signatures in the taxonomic compositions of PD-RBD(+)

An *Enterobacteriaceae* bloom is associated with a disruption in the gut microbiome balance, commonly referred to as dysbiosis [83, 84]. Given that *Escherichia*, which belongs to *Enterobacteriaceae*, was found to be enriched in PD-RBD(+) (Fig. 2, S1, and S2), we investigated whether the taxonomic composition of the gut microbiome in PD-RBD(+) is suggestive of dysbiosis. Notably, the model fit scores for PD-RBD(+) in the enterosignature analysis (see “Materials and methods” section) [44] were markedly lower than those for the HC (Wilcoxon rank-sum test with Holm-Bonferroni correction, q value = 0.033) (Fig. S3), suggesting a dysbiotic state in PD-RBD(+). No significant disparities in the model fit score were found in PD-RBD(-) (q value = 0.32).

Distinct functional characteristics in the gut microbiome of early-stage PD-RBD(+)

To identify the functional characteristics of each group, we utilized DA based on KEGG orthology (KO) functional profiles (Additional file 3). Among the total of 5817

KOs, PD-RBD(+) showed marked functional differences compared to HC (373 enriched and 296 depleted KOs) and PD-RBD(-) (295 enriched and 5 depleted KOs). In contrast, PD-RBD(-) compared to HC resulted in only 23 significantly different KOs (Fig. 3A). Of the significantly altered KOs in PD-RBD(+) when in comparison with HC and PD-RBD(-), 203 KOs were consistently enriched in PD-RBD(+), corresponding to 54.4% of the KOs enriched compared to HC and 51.3% compared to PD-RBD(-) (Fig. 3B; top panel). For the depleted KOs, although only 5 were significantly decreased in PD-RBD(+) compared to PD-RBD(-), 3 of these overlapped with the HC comparison, representing 60% of the total depleted KOs in PD-RBD(-) (Fig. 3B; bottom panel). Overall directions of functions enriched or depleted in PD-RBD(+) when compared to HC and PD-RBD(-) exhibited a similar trend (Spearman's $\rho = 0.69$, p value < $2.2e-16$) (Fig. 3C).

By mapping differential functions to the KEGG pathway, we found that the enriched functions in PD-RBD(+) were associated with the “Biofilm formation–*Escherichia coli*” pathway (map02025) (Fig. 3 D and E). The depleted functions were related to the “Amino sugar and nucleotide sugar metabolism pathway” (map00520) when compared to both HC and PD-RBD(-) (Fig. 3C), as well as “Peptidoglycan biosynthesis” (map00550), and “Starch and sucrose metabolism” (map00500) pathways when compared to HC (Fig. 3D and E). Detailed explanations of these functional results are provided in the subsequent sections.

Augmentation of the *E. coli* biofilm pathway in the gut of early-stage PD-RBD(+)

In PD-RBD(+), among the genes associated with *E. coli* biofilm formation, we found significant increases in the abundance of curli operon genes including *csgD* (a master regulator of biofilm formation) and *csgE* (curli production assembly/transport component) when compared to HC, and *csgA* (curli major subunit) when compared to PD-RBD(-) (Fig. 4A). Additionally, *ydaM*, which positively regulates the *csgD* gene, was enriched in PD-RBD(+) compared to both HC and PD-RBD(-). We also observed significant enrichment of *bcsA* and *bcsB* in PD-RBD(+)

(See figure on next page.)

Fig. 2 Differential abundance analyses reveal gut microbiome differences in PD-RBD(+) compared to PD-RBD(-) and HC. **A** Overall results of pairwise DA analyses utilizing shotgun metagenome data. Rows were hierarchically clustered using the complete linkage method. Taxa referenced in the main text are emphasized in bold. **B, C** Taxa (**B**) enriched or (**C**) depleted in PD-RBD(+) compared to PD-RBD(-) and/or HC as identified by the shotgun metagenome data at the genus level. **D** Taxa enriched in PD-RBD(-) than PD-RBD(+) or HC. **E** Scatter plot depicts the results of DA analyses comparing PD-RBD(+) with PD-RBD(-) (x-axis) and with HC (y-axis). Positive values on both axes represent a positive correlation with PD-RBD(+), while negative values imply a reverse association. The overall results illustrate a substantial positive correlation, suggesting a similar association of taxa with PD-RBD(+) compared to PD-RBD(-) and HC. Red and green represent the taxa depicted in (**B**) and (**C**), respectively. $q < 0.1$; * $q < 0.05$; ** $q < 0.01$; *** $q < 0.001$. *ns* not significant, ρ Spearman's rank correlation coefficient, *PD* Parkinson's disease, *RBD* rapid eye movement sleep behavior disorder, *HC* healthy control, *DA* differential abundance, *RA* relative abundance

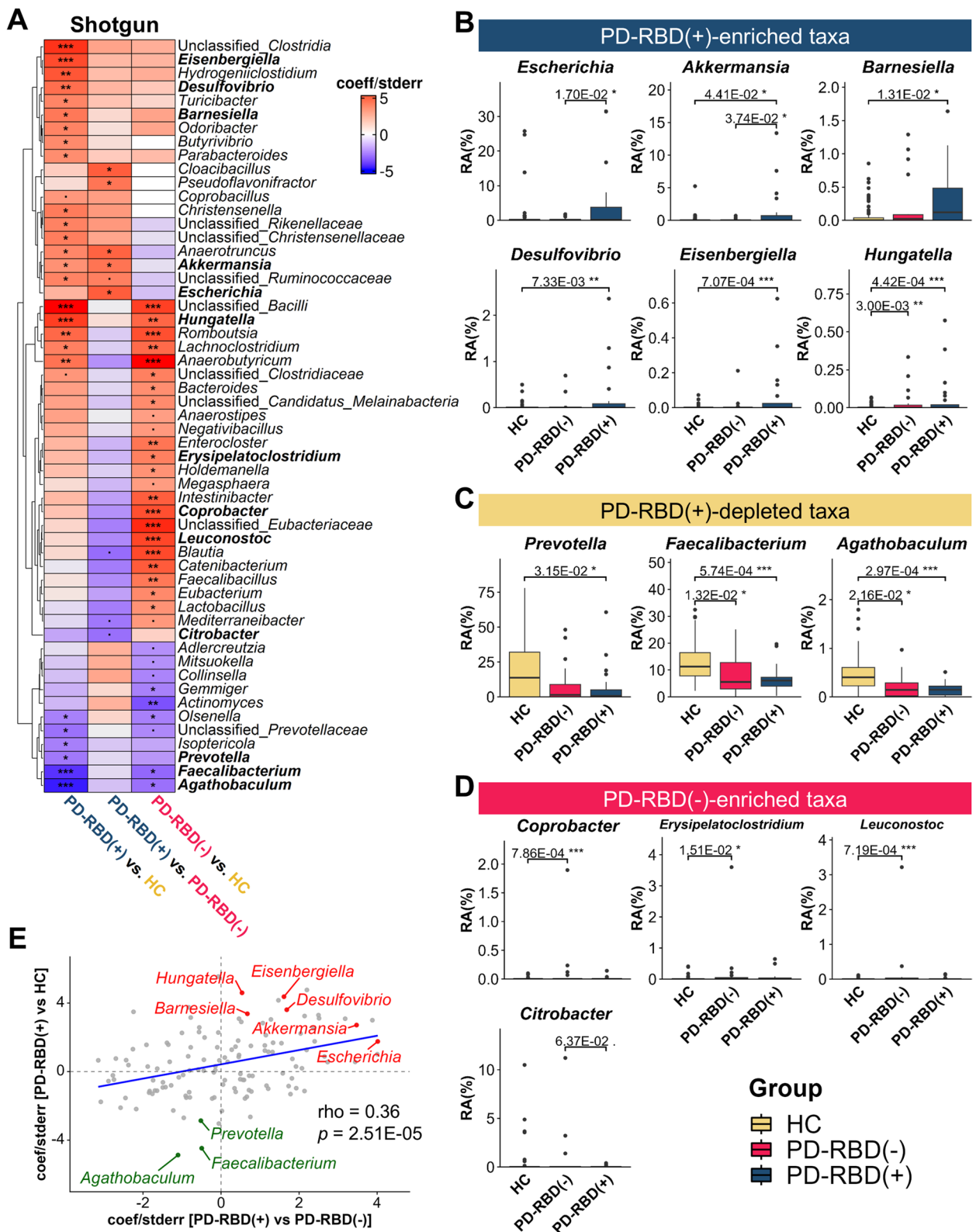


Fig. 2 (See legend on previous page.)

compared to those in HC and/or PD-RBD(−) (Fig. 4A). These genes contribute to the production of cellulose, an essential component of biofilms that confers enhanced cohesion and elasticity [85–87].

Previous studies [11, 69] have highlighted that the capacity of bacterial curli to foster the aggregation of alpha-synuclein varies based on the amyloidogenic potential of CsgA, which is dictated by its amino acid sequence. This suggests that the qualitative property (amino acid sequence) of CsgA is as important as the quantitative property (gene abundance) in explaining its association with PD pathology. In light of this evidence, we analyzed the qualitative aspects of the curli pathway. First, we investigated whether the taxa involved in the curli biofilm pathway varied among groups. In PD-RBD(+), the genus *Escherichia* largely accounted for the taxonomic contribution to the curli and cellulose production pathway (Fig. S4). However, in PD-RBD(−) and HC, the genera *Citrobacter* and *Enterobacter* also contributed to the biofilm pathway, comparable to or even exceeding the contribution of *Escherichia*, indicating potential heterogeneity of the curli biofilm pathway in these groups. To further explore the qualitative properties of CsgA—the actual component that cross-seeds alpha-synuclein—we constructed metagenome-assembled genomes (MAGs) (Fig. S5) and identified the *csgA* gene in a total of 43 *Enterobacteriaceae* genomes (comprising 30 *Escherichia*, 8 *Citrobacter*, 4 *Enterobacter*, and 1 UBA7405 genomes). Among these, CsgA sequences of *Escherichia* were distinct from those of other *Enterobacteriaceae* members (Fig. S6A). In accordance with previous reports [69, 88, 89], all CsgA sequences obtained from the current study demonstrated conserved repeat regions R1–R5 with consensus sequence Gln-X₄-Asn-X₅-Gln (Figs. 4B and S6B). However, in the gatekeeper residues, which modulate aggregation efficiency of CsgA, heterogeneity across taxonomy was observed (Figs. 4B and S6B). Given that the CsgA gatekeeper residues of *Citrobacter* are causally linked to a markedly limited alpha-synuclein aggregation ability [69], suggesting that qualitative properties in addition to abundance of genes are also noteworthy in a clinical context.

Depletion of the UDP-GlcNAc synthesis and recycling pathway in early-stage PD-RBD(+)

We revealed a significant depletion of the uridine diphosphate *N*-acetylglucosamine (UDP-GlcNAc) biosynthesis and recycling pathway (Fig. 5A)—a subpathway related to the amino sugar and nucleotide sugar metabolism (map00520) and the peptidoglycan biosynthesis (map00550) pathways—in the gut microbiome of PD-RBD(+) compared to those in both HC and PD-RBD(−) (Fig. 5B). Particularly, the *glmM* and *glmU* genes, which encode phosphoglucosamine mutase (converting D-glucosamine 6-phosphate [GlcN-6P] to D-glucosamine 1-phosphate [GlcN-1P]) and a bifunctional UDP-GlcNAc pyrophosphorylase/glucosamine-1-phosphate *N*-acetyltransferase (synthesizing UDP-GlcNAc from GlcNAc-1P), respectively, were significantly decreased in PD-RBD(+). Further, the abundance of *nagE*, which encodes the *N*-acetylglucosamine (GlcNAc)-specific sugar phosphotransferase system EIICBA component (uptake extracellular GlcNAc), was also significantly depleted in PD-RBD(+) compared with HC and/or PD-RBD(−) (Fig. 5B). These genes were predominantly associated with gram-positive bacteria, such as *Faecalibacterium*, *Bifidobacterium*, *Blautia*, and *Collinsella* (Fig. 5B). UDP-GlcNAc, synthesized by GlmM and GlmU, serves as a building block for peptidoglycan synthesis and is subsequently released into the environment in the form of GlcNAc during the cell wall turnover process [90]. These environmental GlcNAc is taken up by NagE and then either recycled for UDP-GlcNAc synthesis or utilized for energy [91]. It also acts as a signaling molecule that modulates various cellular processes. For instance, environmental GlcNAc inhibits the expression of curli genes in *E. coli* [92]. Given the observed depletion of the UDP-GlcNAc synthesis/recycling pathway in PD-RBD(+), environmental GlcNAc is speculated to be scarce in PD-RBD(+), potentially fostering a favorable condition for biofilm formation by bacteria.

Inverse relationship between biofilm formation and the UDP-GlcNAc synthesis/recycling pathway

We observed a significant negative correlation between *glmU*, an essential gene for UDP-GlcNAc synthesis, and

(See figure on next page.)

Fig. 3 Distinct functional characteristics of PD-RBD(+) compared to PD-RBD(−) and HC. **A** Bar plot displaying the counts of differentially abundant KEGG orthology (KO) across the group comparisons. The orientation and color of the bars signify which group the KOs are enriched in. **B** Venn diagrams illustrate the counts of differentially abundant KOs identified in the DA analyses comparing PD-RBD(+) with both PD-RBD(−) with HC. **C** Scatter plot illustrates the results of DA analyses of functional profiles comparing PD-RBD(+) with PD-RBD(−) (x-axis) and HC (y-axis). Positive values on both axes denote a positive association with PD-RBD(+), while negative values suggest an inverse one. Red represents genes engaged in Biofilm formation–*Escherichia coli* pathway, while green indicates those involved in the UDP-GlcNAc synthesis/recycling pathway. **D, E** Results of KEGG enrichment analyses using differentially abundant KOs in PD-RBD(+) compared to **(D)** HC and **(E)** PD-RBD(−). Only results with adjusted $p < 0.1$ are presented. The pathways discussed in the main text are emphasized in bold. *PD* Parkinson's disease, *RBD* rapid eye movement sleep behavior disorder, *HC* healthy control, *KEGG* Kyoto Encyclopedia of Genes and Genomes, ρ Spearman's rank correlation coefficient

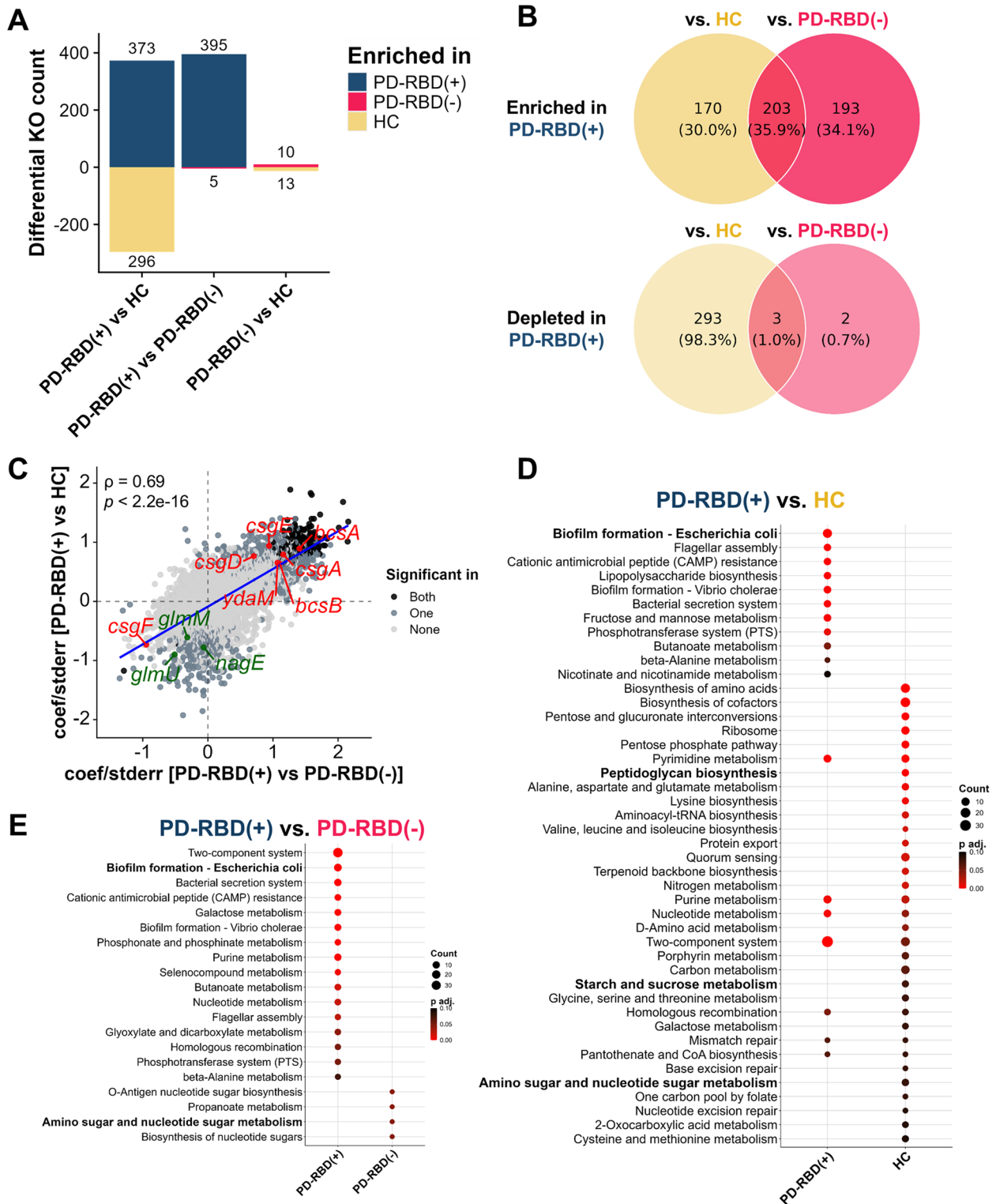


Fig. 3 (See legend on previous page.)

csgD, a master regulator of biofilm formation (Spearman's $\rho = -0.32$, p value = $4.00E-4$) (Fig. 5C). We also identified overall negative correlations between the genes involved in biofilm formation and those in UDP-GlcNAc synthesis and recycling pathways (Fig. S7A). Notably, abundances of genes associated with UDP-GlcNAc production and recycling were negatively correlated (q value < 0.05) with those of biofilm-producing *Escherichia* and *Klebsiella* (Fig. S7B). Particularly, *Escherichia* was enriched in PD-RBD(+) (Figs. 2, S1, and S2). However, the UDP-GlcNAc synthesis and recycling pathway showed a positive correlation with *Faecalibacterium*, *Agathobaculum*, and *Fusicatenibacter* (Fig. S5B)—most of which were depleted in PD-RBD(+) (Figs. 2, S1, and S2). To further validate the general trend of a negative correlation between biofilm formation and the UDP-GlcNAc synthesis/recycling pathways, we analyzed a large-scale PD shotgun study from Wallen et al. (see “Materials and methods” section) [40]. This large cohort study also demonstrated a significant negative correlation (q value < 0.05) for the genes involved in these pathways (Fig. S8), thereby confirming the negative correlation observed in our dataset.

To investigate a relationship between the distribution of microbial genes, *glmU* and *csgD*, and the host disease status, all patients were categorized into four types based on the average CLR abundance of *glmU* and *csgD*: *glmU*-High/*csgD*-High, *glmU*-High/*csgD*-Low, *glmU*-Low/*csgD*-High, and *glmU*-Low/*csgD*-Low (Fig. 5D). There was a significant discrepancy in the distribution of types between HC and PD-RBD(+) (Fisher's exact test: q value = $8.8E-0.3$). No significant differences were observed between PD-RBD(+) and PD-RBD(-) (q value = 0.35), nor between HC and PD-RBD(-) (q value = 0.69). In particular, *csgD*-High/*glmU*-Low type was the most prevalent in the PD-RBD(+). Consequently, given that the environmental GlcNAc downregulates the biofilm-associated genes in *E. coli* [92], the UDP-GlcNAc synthesis and recycling pathway might partially contribute to PD pathogenesis by modulating the formation of detrimental bacterial biofilms.

CAZyme properties in early-stage PD-RBD(+) are biased toward mucin degradation

Carbohydrate-active enzyme (CAZyme) is a group of enzymes that break down, modify, and synthesize complex carbohydrates such as host glycans in the gastrointestinal tract, thereby affecting host health [93]. Previous studies reported that diminished mucus layer is prone to implantation of opportunistic pathogens, such as *E. coli*, thereby leading to infection and inflammation [94–96]. Given that the mucin-degrading bacteria, *Akkermansia* and *Barnesiella*, were enriched in PD-RBD(+) (Figs. 2, S2, and S3), we examined whether CAZyme property of PD-RBD(+) is also functionally altered compared to other groups. We analyzed the CAZyme profiles using MAGs reconstructed from the current dataset (see Methods and Fig. S5), and compared CAZyme composition across groups based on the DA (Additional file 3). In the comparison of PD-RBD(+) and HC, we identified 38 HC-enriched CAZymes and 15 PD-RBD(+)-enriched CAZymes (Fig. 6A). Among the 38 HC-enriched CAZymes, 23 (60.5%) were known for primarily degrading dietary fiber, whereas a relatively small portion of the CAZymes, i.e., 3 (7.9%), were targeting host mucin. In contrast, of the 15 PD-RBD(+)-enriched CAZymes, only 1 (6.7%) CAZyme targeted dietary fiber, while 3 (20%) were known to degrade host mucin, suggesting a notable functional shift towards mucin degradation in PD-RBD(+). This biased capability toward mucin degradation over fiber based on significantly different CAZymes was further statistically tested (Fisher's exact test: p value = $3.7E-4$) (Fig. S9A). Three CAZymes were significantly enriched in PD-RBD(-) compared to HC, although their involvement with fiber or mucin degradation remains unknown so far (Fig. S9B). No significant differences were observed between PD-RBD(+) and PD-RBD(-).

The target substrate profiles of the differentially abundant CAZymes further reaffirmed the preference of PD-RBD(+)-enriched CAZymes toward host mucin. Most of the HC-enriched CAZymes primarily targeted dietary

(See figure on next page.)

Fig. 4 Differential gene abundances and diverse curli sequence characteristics in the gut microbiome of patients with PD and HC. **A** The abundance of the genes involved in the biofilm formation—*E. coli* pathway (KEGG pathway map02025) was found to be significantly elevated in PD-RBD(+) compared to those in HC and/or PD-RBD(-). The *csgD* gene (red box) serves as a master regulator for the biofilm formation pathway, and the *ydaM* gene is an upregulator of *csgD*. CsgD facilitates curli production by activating the *csgBAC* (encoding curli subunits and a curli chaperone) and *csgEFG* (encoding a curli secretion system) operons (orange box). Furthermore, CsgD enhances the expression of *adrA*, which in turn triggers the cellulose synthase operon *bcsABZC* through the signaling molecule c-di-GMP (blue box). Both curli and cellulose constitute bacterial biofilms. The curli fibrils produced during this process promote pathologic aggregation of alpha-synuclein. **B** The sequence logo of curli major subunit CsgA sequences retrieved from the MAGs or from the reference DB (UniProt P28307 for *E. coli* K12 and A0A9Q7ZLG0 for *Citrobacter youngae*). The multiple sequence alignment used to build the sequence logo is visualized in Fig. S6B (Additional file 1). All CsgA sequences exhibited conserved repeat regions (R1–R5 indicated by black arrows; only R2–R4 are shown in this figure). The gatekeeper residues are highlighted and indicated by purple arrows. $q < 0.1$; * $q < 0.05$. PD Parkinson's disease, RBD rapid eye movement sleep behavior disorder, HC healthy control, KEGG Kyoto Encyclopedia of Genes and Genomes, RA relative abundance, MAG metagenome-assembled genome

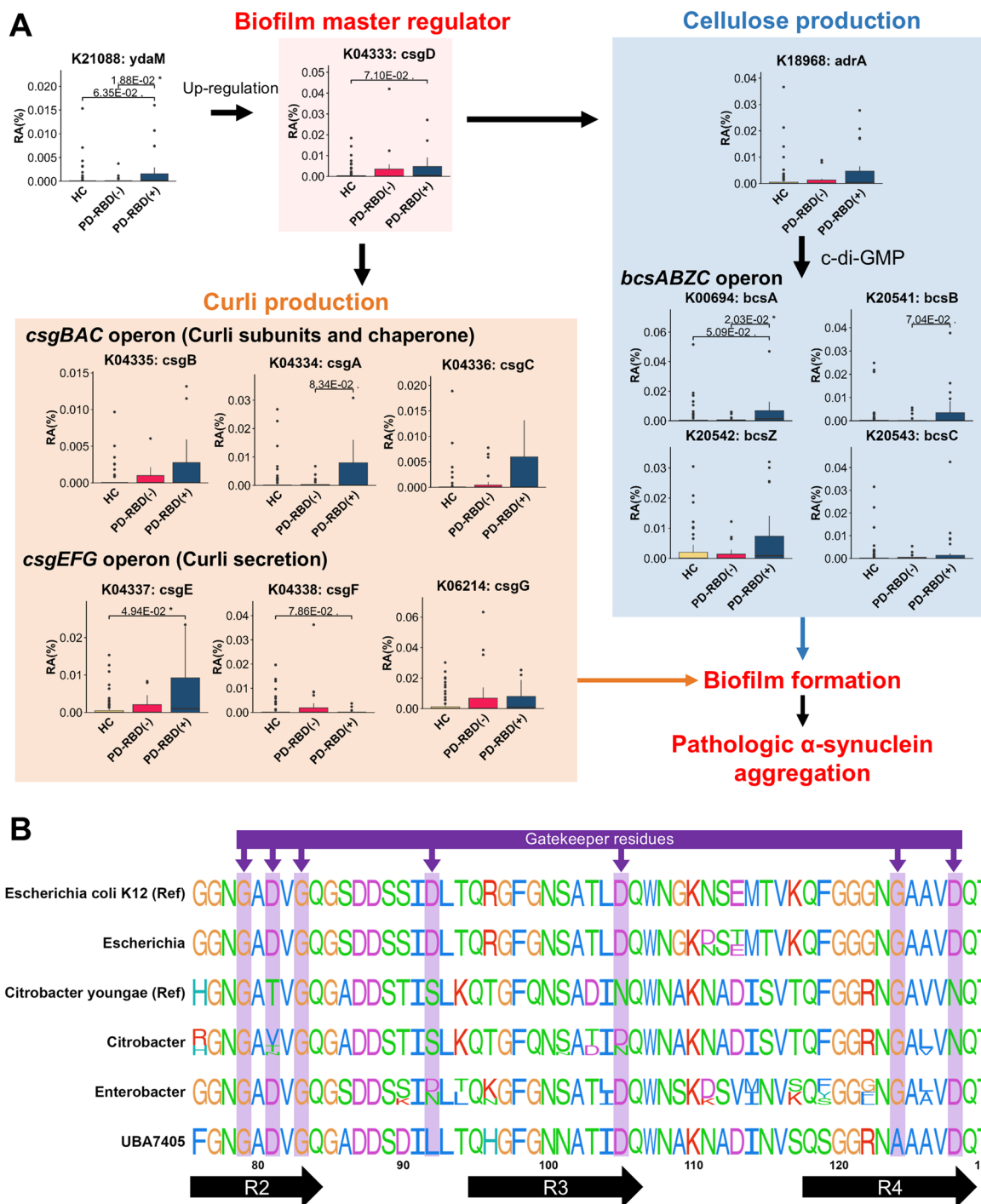


Fig. 4 (See legend on previous page.)

fibers such as xylan, pectin, beta-glucan, cellulose, arabinan, and starch (Fig. 6B). In contrast, PD-RBD(+)-enriched CAZymes exhibited a stronger preference for host-derived carbohydrates, such as host glycans and human milk polysaccharides (HMOs) (Fig. 6B). We further investigated the relationship between the gut

microbiota and CAZymes by assessing the contribution of bacterial taxa to the differentially abundant CAZymes (Fig. 6C). We further observed that *Prevotella*, which is sensitive to dietary fiber [76, 97], was a predominant contributor to HC-enriched CAZymes. Its contribution was roughly proportional to the magnitude of the coefficient

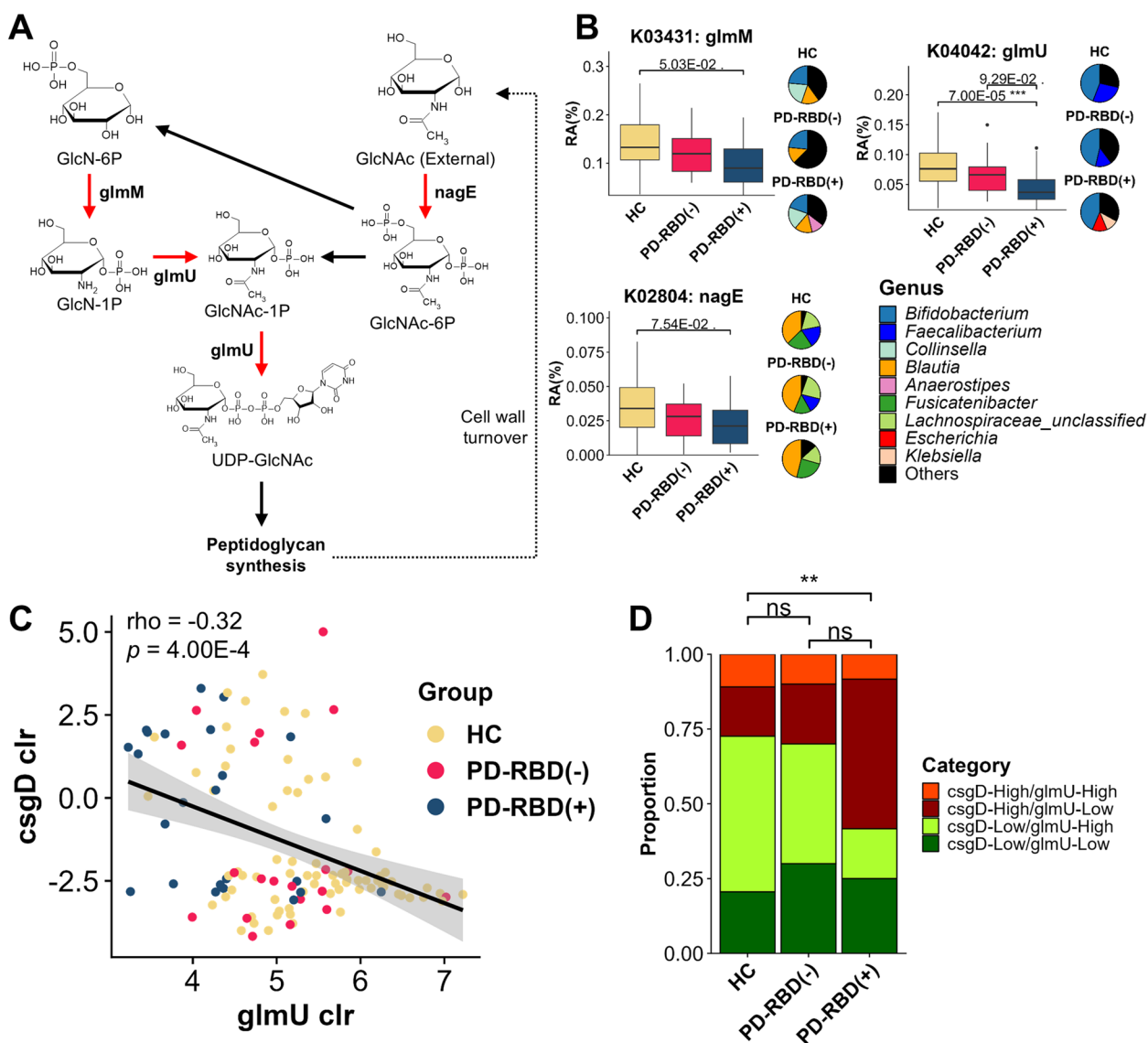


Fig. 5 The UDP-GlcNAc synthesis/recycling pathway is depleted in PD-RBD(+) and negatively correlated with bacterial biofilm formation. **A** Schematic representation of the UDP-GlcNAc synthesis and recycling pathway, which is related to the amino sugar and nucleotide sugar metabolism (KEGG pathway map00520) and peptidoglycan biosynthesis (map00550) pathways. Solid red arrows denote reactions catalyzed by enzymes encoded by genes exhibiting significant differences in the DA analyses, whereas solid black arrows signify reactions facilitated by those without significant differences. **B** Relative abundances of significantly different genes marked by solid red arrows in (A). Pie charts represent taxonomic contributions to each gene across groups. **C** Scatter plot of centered log-ratio (clr) transformed abundances for *csgD* and *glmU* genes, which are essential for biofilm formation and UDP-GlcNAc synthesis, respectively. These genes show a negative correlation ($\rho = -0.32$, $p = 4.0E-4$). **D** Distribution of the four subject categories based on the clr-transformed abundances of *csgD* and *glmU* genes across groups. Fisher's exact test was used for statistical analysis. $q < 0.1$; $*q < 0.05$; $***q < 0.001$ for DA analysis. $**p < 0.01$ for Fisher's exact test. *ns* not significant, ρ Spearman's rank correlation coefficient, *GlcN-6P* glucosamine 6-phosphate, *GlcN-1P* glucosamine 1-phosphate, *GlcNAc* *N*-acetylglucosamine, *GlcNAc-6P* GlcNAc 6-phosphate, *GlcNAc-1P* GlcNAc 1-phosphate, *UDP-GlcNAc* uridine diphosphate-GlcNAc, *DA* differential abundance, *PD* Parkinson's disease, *RBD* rapid eye movement sleep behavior disorder

in the HC-enriched CAZymes in the DA (Fig. 6 A and C). Other fiber-associated bacteria *Faecalibacterium* and *Fusicatenibacter* [75, 97, 98], and neuroprotective bacteria *Agathobaculum* [78]—all of which displayed positive correlations with the UDP-GlcNAc synthesis

and recycling pathway (Fig. S5B)—also contributed substantially to HC-enriched CAZymes (Fig. 6C). In contrast, UBA1829 and *Akkermansia*, both of which belong to phylum Verrucomicrobiota, predominantly contributed to the PD-RBD(+)-enriched CAZymes (Fig. 6C).

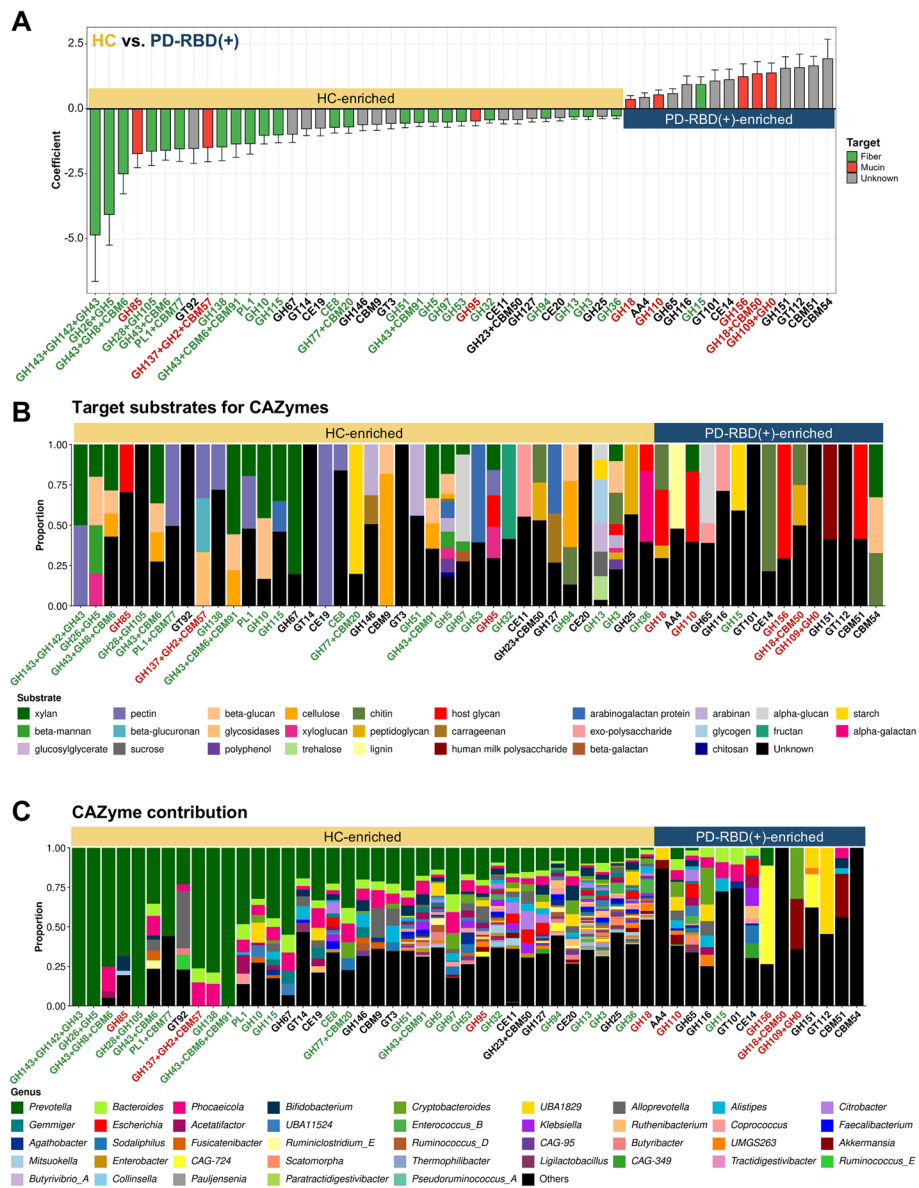


Fig. 6 Differentially abundant CAZymes between PD-RBD(+) and HC, and the associated substrates and taxa. **A** A waterfall plot of DA analysis comparing the CAZyme profiles between PD-RBD(+) and HC. Only significant results are shown. CAZymes targeting dietary fibers and host mucins are indicated by green and red colors, respectively. Error bars represent the standard error from the model. **B, C** (B) Target substrate and (C) taxonomic contribution profiles of differentially abundant CAZymes. The order of CAZymes along the x-axis is consistent with that in (A). *GH* glycoside hydrolase, *GT* glycosyl transferase, *PL* polysaccharide lyase, *CE* carbohydrate esterase, *AA* auxiliary activity, *CMB* carbohydrate-binding module, *PD* Parkinson’s disease, *RBD* rapid eye movement sleep behavior disorder, *HC* healthy control, *DA* differential abundance

Bacteroides, *Phocaeicola*, and *Cryptobacteroides*, all of which belong to *Bacteroidales*, exhibited an even contribution across most of the differentially abundant CAZymes (Fig. 6C).

Consequently, the gut microbiome of PD-RBD(+) exhibited a marked functional preference for mucin degradation over that for fiber degradation in their CAZymes profile. Excessive degradation of host mucin by the gut

microbiome could increase susceptibility to pathogenic infections and gut inflammation [94–97].

Discussion

In this study, we discovered that the gut microbiome in PD-RBD(+) (patients with PD and premotor RBD) maintained a distinct composition regardless of disease stage, that of PD-RBD(–) (patients with PD without

premotor RBD) began with a composition similar to HC but diverged toward PD-RBD(+) as the disease advanced. Notably, gut bacteria associated with host mucin degradation (*Akkermansia* and *Barnesiella*) and pathogenic biofilm formation (*Escherichia*) were increased in PD-RBD(+). Fiber intake-associated taxa, *Prevotella*, *Faecalibacterium*, and *Agathobacter* were decreased in PD-RBD(+). These were further supported by functional analysis: biased mucin degrading capacity of CAZymes rather than fiber degradation and increased biofilm master regulator *csfD* in PD-RBD(+). Genes related to biofilm formation were negatively correlated with UDP-GlcNAc synthesis/recycling pathways; this was further validated in a separate cohort [40], suggesting the inhibitory role of the UDP-GlcNAc pathway on biofilm formation (Fig. 7).

Most of our taxonomy findings are consistent with previous studies investigating the gut microbiome in idiopathic RBD, PD, and PD with premotor RBD [8, 13–15, 17, 40, 62–65, 72, 73], which have reported an enrichment of *Akkermansia*, *Eisenbergiella*, *Desulfovibrio*, *Hungatella*, and *Barnesiella*, and a decreased abundance of *Prevotella*, *Faecalibacterium*, and *Agathobacter*. Notably, *Coprobacter*, *Erysipelatoclostridium*, and *Leuconostoc*—rarely reported in studies of PD [82, 99]—were observed to increase in PD-RBD(−). Four studies [40, 62, 63, 72] employing shotgun metagenome sequencing implicating functional insights, with three reporting alterations in carbohydrate metabolism pathways [40, 62, 72] and one study [40] indicating an increase in curli production in patients. Only one of these studies included a PD-RBD(−) group [15]; however, due to the limitations of 16S rRNA gene amplicon sequencing, it presented limited functional implications based on predicted functional profiles. Additionally, only one of the shotgun metagenomics studies accounted for RBD status [62]. In this context, our study addresses an important knowledge gap by providing a comprehensive functional perspective on early-stage PD with premotor RBD, thereby extending our understanding of these associations in addition to prior findings.

The microbial composition of PD-RBD(+) exhibited a unique profile compared to that of HC or PD-RBD(−); this characteristic was stable during the disease progression. However, the microbial composition of PD-RBD(−) was initially close to HC but gradually changed toward that of PD-RBD(+). A key distinguishing feature of the body-first PD is the presence of idiopathic REM sleep behavior disorder (RBD) several years prior to the PD diagnosis, indicating pathology propagation from the subcoeruleus complex in the pons to the substantia nigra. In brain-first type, central nervous degeneration occurs independently of RBD. Thus, the relatively stable

microbiome composition observed in PD-RBD(+), and similar gut microbiome profile between PD and idiopathic RBD [13–15] may suggest that disease progression in the gut may have reached an advanced stage, leaving little room for further change. In contrast, the relatively dynamic shifts in the gut microbiome composition according to disease stages in PD-RBD(−) may suggest that pathological processes in the gut could be affected by disease progression. Although we cannot definitively determine the routes involved—whether through the spread of alpha-synuclein or the immune system—these findings emphasize the potential role of the gut microbiota in the pathophysiology of PD and highlight the need for further investigation.

The genus *Escherichia*, which is enriched in PD-RBD(+), is recognized for its production of the amyloid fiber protein curli, which is an essential component for biofilm formation [70, 87, 100]. Recently, various in vivo studies have underscored the putative contributing role of curli protein in PD pathogenesis, particularly in facilitating alpha-synuclein aggregation and inflammation in the gut and brain [10–12, 68–70]. In the current study, we demonstrated the enrichment of genes involved in the biofilm formation pathway in PD-RBD(+) (Fig. 4). Additionally, genes involved in the synthesis of cellulose—another pivotal biofilm component that confers enhanced cohesion and elasticity to the bacterial biofilm [85–87]—were also enriched in PD-RBD(+) compared to those in PD-RBD(−) and/or HC. Enrichment of these biofilm-associated genes in the metagenomes was largely accounted for by the genus *Escherichia*. Thus, the detrimental effects of curli proteins from *Escherichia* biofilms on PD pathophysiology may be confined exclusively to PD-RBD(+) and be independent of the PD-RBD(−). This could elucidate the rapid progression factors of clinical symptoms in PD with premotor RBD potentially via increased adherence to host cells of *Escherichia* and alpha-synuclein cross-seeding, both of which could consistently incite inflammation.

In PD-RBD(+), carbohydrate-degrading ability of the gut microbiome shifts from primarily degrading dietary fibers to degrading host mucin [94, 95]. This is in line with taxonomy findings, which showed significant enrichment of the genera *Akkermansia*, *Barnesiella*, *Desulfovibrio*, and *Hungatella* in PD-RBD(+), along with depletion of *Prevotella*, *Faecalibacterium*, and *Agathobacter*. *Akkermansia* and *Barnesiella* specialize in mucin degradation, and *Desulfovibrio* is known to use the sulfate liberated from mucin [71]. *Hungatella* was also recently reported as capable of degrading host glycans [101]. In contrast, *Prevotella*, *Faecalibacterium*, and *Agathobacter* are known to be associated with fiber intake. Excessive mucin degradation leads to gut barrier dysfunction with

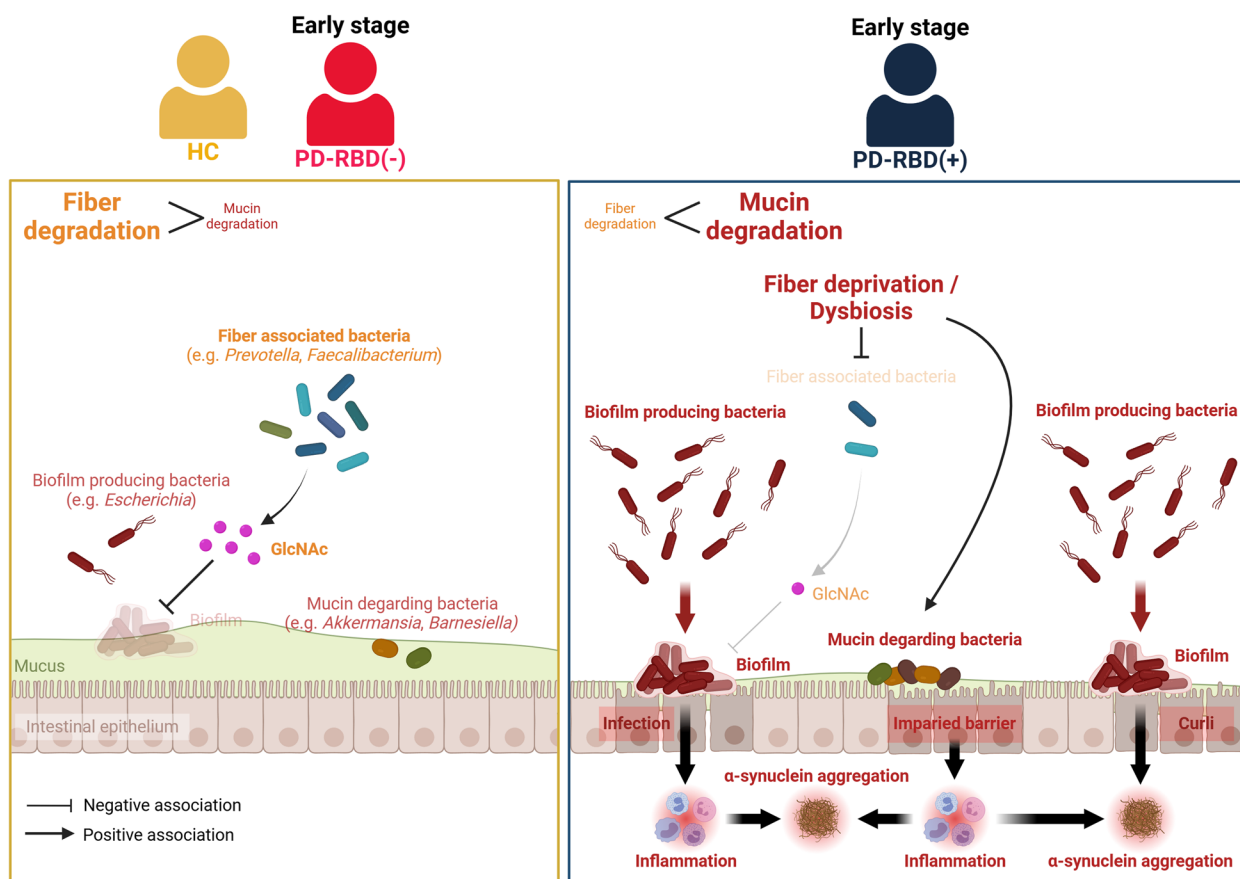


Fig. 7 Graphical summary of the current study. Left panel: In both HC and early-stage PD-RBD(−) compared to early-stage PD-RBD(+), the gut microbiome tends to favor degradation of dietary fibers over host mucin. In line with this, the abundance of fiber-associated bacteria (i.e., *Prevotella*, *Faecalibacterium*, and *Agathobacter*) is increased, whereas that of mucin degradation-associated bacteria (i.e., *Akkermansia*, *Barnesiella*, and *Desulfovibrio*) is decreased. In HC and PD-RBD(−), fiber-associated bacteria are associated with enhanced capability to discharge *N*-acetylglucosamine (GlcNAc) into the environment, which in turn suppresses biofilm formation by biofilm-producing bacteria (i.e., *Escherichia*). Right panel: Conversely, in early-stage PD-RBD(+) compared to both in HC and early-stage PD-RBD(−), the gut microbiome shows a preference for degrading host mucin over dietary fibers. Correspondingly, abundance of fiber-associated bacteria is reduced, and that of mucin degradation-associated bacteria is increased. The reduction in fiber-associated bacteria may lead to a scarcity of GlcNAc, thereby facilitating easier biofilm formation by bacteria. Consequently, these characteristics of PD-RBD(+) may be associated with increased susceptibility to infection and inflammation, potentially contributing to the exacerbation of PD pathophysiology, such as alpha-synuclein aggregation. *PD* Parkinson’s disease, *RBD* rapid eye movement sleep behavior disorder, *HC* healthy control. Created with BioRender.com

a thinner mucus layer, thereby predisposing the host to inflammatory conditions such as pathogen infection [94, 95, 102] and inflammatory diseases [97]. These inflammatory conditions have been reported to be associated with an increased risk of PD [103–107].

Although these similar functional and taxonomic changes have been reported under fiber deprivation conditions [76, 94, 95, 98], dietary surveys in our study confirmed that there was no actual difference in fiber consumption between PD-RBD(+) and PD-RBD(−), with median fiber intake of 34–36 g even exceeding the recommended amount 25 g [108] (Additional file 1: Supplementary Table S1). The diet may have shifted toward a

healthier pattern following PD diagnosis. Consequently, dietary habits during the critical period of pathology formation, few years prior to PD diagnosis, may not have been accurately reflected. The long-term effects of dietary changes on gut microbiota are unclear, as evidence suggests that short-term dietary changes may have less impact on gut microbiota composition than habitual diet patterns [108]. Also, gut dysbiosis of PD would not respond well to fiber-rich diet. While the mechanistic relationship remains unknown in the current study, these findings suggest that restoring normal gut microbiome balance through dietary interventions alone may be challenging in a dysbiotic context [108]. Investigating

strategies to address dysbiosis in conjunction with dietary interventions could be essential in developing effective treatments for diseases associated with gut microbiome imbalances.

Signatures of gut dysbiosis were apparent in PD-RBD(+). *Escherichia*, infamously associated with dysbiosis [83, 84], was enriched in PD-RBD(+). Additionally, a significantly lower ES model fitness was observed in PD-RBD(+). This indicates a deviation from typical gut microbiome compositions and an association with the causative events of dysbiosis [44]. Importantly, gut dysbiosis is known to be positively associated with increased gut inflammation and permeability [70, 83, 84, 109], which have been previously reported in PD [105, 107, 110–112]. Hence, assessing and comparing intestinal inflammation and permeability between PD-RBD(+) and PD-RBD(-) may provide further insights into the role of detrimental gut conditions in PD pathogenesis.

Depletion of the UDP-GlcNAc synthesis and recycling pathway was another prominent feature of the gut microbiome in PD-RBD(+). UDP-GlcNAc serves as a precursor of cell wall peptidoglycan in bacteria. Once incorporated into cell wall peptidoglycans as GlcNAc, it is eventually released into the environment via active cell wall turnover, thereby elevating the level of environmental GlcNAc [90, 91]. Environmental GlcNAc might play a role in PD pathogenesis through two potential mechanisms in the gut: Firstly, it modulates the biofilm formation of intestinal bacteria. GlcNAc-6P, the intracellularly imported form of environmental GlcNAc, downregulates the biofilm-associated genes in *E. coli* [92]. Thus, intestinal GlcNAc could act as an inhibitory molecule for biofilm formation by pathogenic bacteria. This is supported by the inverse relationships between the genes involved in the biofilm formation and the UDP-GlcNAc synthesis/recycling pathways observed both in our data and another large-scale cohort [40]. Secondly, it modulates host O-GlcNAcylation profiles. O-GlcNAcylation is a type of post-translational modification, in which the GlcNAc moiety from UDP-GlcNAc is covalently attached to Ser/Thr residues on proteins. Recent studies have underscored the importance of O-GlcNAcylation in PD pathogenesis. Specifically, O-GlcNAcylation of alpha-synuclein prevents its pathogenic aggregation and mitigates neuronal cell death and motor deficits in a PD animal model [113, 114]. Notably, exogenous GlcNAc can increase intracellular UDP-GlcNAc and O-GlcNAcylation levels [91, 115, 116]. Hence, it is plausible that the intestinal GlcNAc originating from the gut microbiome and dietary sources impacts the host O-GlcNAcylation profiles. Collectively, the scarcity of GlcNAc in the gut of PD-RBD(+) might provide favorable circumstances for biofilm formation by gut pathobionts like *E. coli*, and alter the host

protein O-GlcNAcylation, which is potentially related to PD pathogenesis.

We found that *Coprobacter*, *Erysipelatoclostridium*, *Leuconostoc*, and *Citrobacter* were positively associated with PD-RBD(-) compared with PD-RBD(+) or HC. *Coprobacter* and *Leuconostoc* are SCFA-producing bacteria, which were positively associated with PD in one study each [79, 80], but not in idiopathic RBD or PD-RBD(+) [13, 62]. Because low abundance of SCFA-producing bacteria is generally associated with PD and its progression [9], the mechanistic explanation about positive relationship between these bacteria and PD necessitates further investigation. *Citrobacter*, another curli-producing gut bacterium, was also enriched in PD-RBD(-). However, in accordance with a previous study [69], we discovered that the gatekeeper residues, crucial for the aggregation and cross-seeding efficiency of CsgA [87], exhibited heterogeneity across genera in our dataset (Figs. 4B, S6). Notably, the CsgA gatekeeper residues in *Citrobacter*, which differ from those in *Escherichia*, confer faster aggregation properties; however, they also confer significantly weaker cross-interactions with alpha-synuclein [67]. Given the limited propensity of *Citrobacter* CsgA for alpha-synuclein cross-seeding, it is unlikely that the enrichment of *Citrobacter* in PD-RBD(-) is associated with intestinal alpha-synuclein aggregation.

This cross-sectional study unveils identifying distinct microbial profiles in the subgroup of PD with premotor RBD, which could contribute to PD pathophysiology via biofilm formation, mucin degradation, and UDP-GlcNAc synthesis. We also demonstrated a negative correlation between the biofilm pathway and UDP-GlcNAc pathway and validated this in an additional large-scale cohort [40]. These findings bear clinical relevance, as they suggest that patients with premotor RBD should be a focus for research and therapeutic interventions targeting the gut microbiome. This insight may potentially lead to the development of new strategies for PD management.

This study contains various limitations. First, the correlation between the gut microbiota composition and PD with premotor RBD symptoms does not establish causation, leaving it uncertain whether they have a direct role in PD pathogenesis. We have identified the microbiome pathways associated with alpha-synuclein formation through functional analysis; future experimental studies are required to validate our findings. Second, the study was cross-sectional, but we tried to show the microbiome patterns of patients with PD according to disease stage. Third, the study does not thoroughly address potential confounding factors that can influence the gut microbiota, such as lifestyle and comorbidities. Fourth, although we identified distinct gut microbiome characteristics in patients with PD based on the presence of premotor

RBD, the sample size of each subgroup, especially when stratified by disease stage, was relatively small. To our knowledge, no previous large-scale study has comprehensively analyzed and publicly shared data considering both premotor RBD status and disease stage in patients with PD. Consequently, determining an appropriate sample size prior to conducting this study was challenging given the available data. We therefore conducted a PERMANOVA power estimation [61] to assess the adequacy of our sample size for key comparisons, which indicated that the current sample size provided sufficient power to detect moderate effect sizes. To obtain more robust and generalizable results, future studies with larger cohorts are warranted.

Conclusions

In conclusion, this study revealed that (1) gut microbiome dynamics in patients with PD according to the disease stage depend on the presence of premotor RBD, and (2) distinct gut microbiome characteristics in patients with early-stage PD-RBD(+). These distinct characteristics include increased pathogenic biofilm formation and host mucin degradation, which could predispose patients to infection and inflammation, thereby contributing to the exacerbation of PD pathophysiology in the gut. Functional analysis revealed a potential link between GlcNAc, which downregulates biofilm formation, and PD pathogenesis, as demonstrated by negative correlations between biofilm formation and UDP-GlcNAc synthesis/recycling pathways observed in this study and validated with data from another large cohort. Overall, our finding underscores the importance of considering disease stage and premotor RBD in gut microbiome studies of patients with PD. Moreover, we consolidated the mechanisms by which the gut microbiome influences PD pathophysiology. These findings may provide a foundation for developing new therapeutic approaches targeting the gut microbiome in PD.

Supplementary Information

The online version contains supplementary material available at <https://doi.org/10.1186/s40168-025-02095-w>.

Additional file 1: Supplementary Fig. S1. Differentially abundant taxa in PD-RBD(+), compared to those in PD-RBD(-) and HC using 16S rRNA gene amplicon data. Supplementary Fig. S2. Differentially abundant species in PD-RBD(+), compared to those in PD-RBD(-) and HC using shotgun metagenome data. Supplementary Fig. S3. Model fit scores of the subjects calculated from the enterosignature analysis across the group. Supplementary Fig. S4. Taxa contributions to the curli and cellulose biofilm formation pathway. Supplementary Fig. S5. Workflow for the metagenome-assembled genome (MAG) analysis. Supplementary Fig. S6. Phylogenetic tree and multiple sequence alignment of curli major subunit CsgA sequences retrieved from MAGs. Supplementary Fig. S7. Correlation analyses among genes involved in biofilm formation and UDP-GlcNAc synthesis and recycling pathways, and the associated taxa. Supplementary

Fig. S8. Validation of the inverse relationship between biofilm formation and the UDP-GlcNAc synthesis/recycling pathway in a large cohort study. Supplementary Fig. S9. Characteristics of enriched CAZymes in PD-RBD(+) and PD-RBD(-) compared to HC. Supplementary Table S1. Comparison of dietary intake between patients with Parkinson's disease (PD) with/without rapid eye movement behavior disorders (RBD) and healthy controls. Supplementary Table S2. PERMANOVA test results between PD-RBD(+) and PD-RBD(-) based on unweighted UniFrac distance with levodopa usage or LEDD as a covariate in each stage. Supplementary Table S3. Linear regression model constructed with Unweighted UniFrac distance from HC to PD-RBD(+) and PD-RBD(-) with covariate age. Supplementary Table S4. Linear regression model constructed with Unweighted UniFrac distance from early-stage to late-stage in PD with covariate age. Supplementary Table S5. Baseline demographics of patients with early Parkinson's disease (PD) with/without rapid eye movement behavior disorders (RBD) and the healthy control (HC). Supplementary Table S6. Baseline demographics of patients with late Parkinson's disease (PD) with/without rapid eye movement behavior disorders (RBD) and the healthy control (HC).

Additional file 2: Table S1. Targets of CAZymes and literature references.

Additional file 3: Data S1. Result of PD-RBD(+) vs. HC from MaAsLin2 analysis at the Genus level on the taxonomy profile of shotgun metagenomics data. Data S2. Result of PD-RBD(+) vs. PD-RBD(-) from MaAsLin2 analysis at the Genus level on the taxonomy profile of shotgun metagenomics data. Data S3. Result of PD-RBD(-) vs. HC from MaAsLin2 analysis at the Genus level on the taxonomy profile of shotgun metagenomics data. Data S4. Result of PD-RBD(+) vs. HC from ANCOM-BC analysis at the Genus level on the taxonomy profile of 16S amplicon data. Data S5. Result of PD-RBD(+) vs. PD-RBD(-) from MaAsLin2 analysis at the Genus level on the taxonomy profile of 16S amplicon data. Data S6. Result of PD-RBD(-) vs. HC from MaAsLin2 analysis at the Genus level on the taxonomy profile of 16S amplicon data. Data S7. Result of PD-RBD(+) vs. HC from MaAsLin2 analysis at the Species level on the taxonomy profile of shotgun metagenomics data. Data S8. Result of PD-RBD(+) vs. PD-RBD(-) from MaAsLin2 analysis at the Species level on the taxonomy profile of shotgun metagenomics data. Data S9. Result of PD-RBD(-) vs. HC from MaAsLin2 analysis at the Species level on the taxonomy profile of shotgun metagenomics data. Data S10. Result of PD-RBD(+) vs. HC from ANCOM-BC analysis on the function profile of shotgun metagenomics data. Data S11. Result of PD-RBD(+) vs. PD-RBD(-) from ANCOM-BC analysis on the function profile of shotgun metagenomics data. Data S12. Result of PD-RBD(-) vs. HC from ANCOM-BC analysis on the function profile of shotgun metagenomics data. Data S13. Result of PD-RBD(+) vs. HC from MaAsLin2 analysis on the CAZyme profile of shotgun metagenomics data. Data S14. Result of PD-RBD(+) vs. PD-RBD(-) from MaAsLin2 analysis on the CAZyme profile of shotgun metagenomics data. Data S15. Result of PD-RBD(-) vs. HC from MaAsLin2 analysis on the CAZyme profile of shotgun metagenomics data.

Acknowledgements

None.

Authors' contributions

Conceptualization, J-YL, S-J, J-WB, SJC. Methodology, J-YL, S-J, J-WB, SJC. Investigation, J-YL, S-J, JL, MC, K-K, SL, HSK, J-WB, SJC. Writing – Original Draft, J-YL, S-J, J-WB, SJC. Writing – Review & Editing, J-YL, S-J, JL, MC, K-K, SL, HSK, J-WB, SJC. Funding Acquisition, SJC and S-J. Supervision, J-WB, SJC. All authors reviewed and approved the manuscript.

Funding

This research was supported by a grant from the Korea Health Technology R&D Project through the Korea Health Industry Development Institute (KHIDI), funded by the Ministry of Health & Welfare, Republic of Korea (grant number: RS-2023-00265820), and the National Research Foundation of Korea (NRF) grant funded by the Korea government (MSIT) (RS-2024-00353952).

Data availability

The datasets generated during the previous study are available in the NCBI (<https://www.ncbi.nlm.nih.gov>) Sequence Read Archive database under the accession numbers PRJNA742875 (16S rRNA gene amplicon data),

PRJNA743718 (shotgun metagenome data), and PRJNA1177354 (16S rRNA gene amplicon and shotgun metagenome data). Public PD metagenome data used in this study was retrieved from PRJNA834801. The analysis scripts and a multiple sequence alignment file of CsgA from MAGs used in this study are available on GitHub (<https://github.com/jylee3247/PD-with-or-without-premotor-RBD-gut-microbiome>) and Zenodo (<https://doi.org/10.5281/zenodo.13987680>). All results from the differential abundance analyses are provided in Additional file 3.

Declarations

Ethics approval and consent to participate

This study was approved by the Asan Medical Center Institutional Review Board (2019–0929) and was performed in accordance with the relevant guidelines and regulations, including the Declaration of Helsinki. All participants provided written informed consent at study enrollment.

Consent for publication

Not applicable.

Competing interests

The authors declare no competing interests.

Author details

¹Department of Biology and Department of Life and Nanopharmaceutical Science, Kyung Hee University, Seoul 02447, Republic of Korea. ²Department of Neurology, Asan Medical Center, University of Ulsan College of Medicine, Seoul 05505, Republic of Korea.

Received: 29 February 2024 Accepted: 17 March 2025

Published online: 30 April 2025

References

- Goedert M, Spillantini MG, Del Tredici K, Braak H. 100 years of Lewy pathology. *Nat Rev Neurol*. 2013;9:13–24.
- Braak H, Del Tredici K, Rüb U, de Vos RA, Jansen Steur EN, Braak E. Staging of brain pathology related to sporadic Parkinson's disease. *Neurobiol Aging*. 2003;24:197–211.
- Stokholm MG, Danielsen EH, Hamilton-Dutoit SJ, Borghammer P. Pathological α -synuclein in gastrointestinal tissues from prodromal Parkinson disease patients. *Ann Neurol*. 2016;79:940–9.
- Stockdale SR, Draper LA, O'Donovan SM, Barton W, O'Sullivan O, Volpicelli-Daley LA, Sullivan AM, O'Neill C, Hill C. Alpha-synuclein alters the faecal viromes of rats in a gut-initiated model of Parkinson's disease. *Commun Biol*. 2021;4:1140.
- Horsager J, Andersen KB, Knudsen K, Skjærbaek C, Fedorova TD, Okkels N, Schaeffer E, Bonkat SK, Geday J, Otto M, et al. Brain-first versus body-first Parkinson's disease: a multimodal imaging case-control study. *Brain*. 2020;143:3077–88.
- Jiang X, Pan Y, Zhu S, Wang Y, Gu R, Jiang Y, Shen B, Zhu J, Xu S, Yan J, et al. Alterations of regional homogeneity in Parkinson's disease with rapid eye movement sleep behavior disorder. *Neuropsychiatr Dis Treat*. 2022;18:2967–78.
- Leclair-Visonneau L, Clairembault T, Coron E, Le Dily S, Vavasseur F, Dalichamp M, Péron Y, Neunlist M, Derkinderen P. REM sleep behavior disorder is related to enteric neuropathology in Parkinson disease. *Neurology*. 2017;89:1612–8.
- Nishiwaki H, Hamaguchi T, Ito M, Ishida T, Maeda T, Kashihara K, Tsuboi Y, Ueyama J, Shimamura T, Mori H, et al. Short-chain fatty acid-producing gut microbiota is decreased in Parkinson's disease but not in rapid-eye-movement sleep behavior disorder. *Msystems*. 2020;5(6):10–128.
- Nishiwaki H, Ito M, Hamaguchi T, Maeda T, Kashihara K, Tsuboi Y, Ueyama J, Yoshida T, Hanada H, Takeuchi I, et al. Short chain fatty acids-producing and mucin-degrading intestinal bacteria predict the progression of early Parkinson's disease. *NPJ Parkinsons Dis*. 2022;8:65.
- Chen SG, Stribinski V, Rane MJ, Demuth DR, Gozal E, Roberts AM, Jagadapillai R, Liu R, Choe K, Shivakumar B, et al. Exposure to the functional bacterial amyloid protein curli enhances alpha-synuclein aggregation in aged Fischer 344 rats and *Caenorhabditis elegans*. *Sci Rep*. 2016;6:34477.
- Samson TR, Challis C, Jain N, Moiseyenko A, Ladinsky MS, Shastri GG, Thron T, Needham BD, Horvath I, Debelius JW, et al. A gut bacterial amyloid promotes alpha-synuclein aggregation and motor impairment in mice. *Elife*. 2020;9:9.
- Schmit KJ, Garcia P, Sciortino A, Aho VTE, Pardo Rodriguez B, Thomas MH, Gerardy JJ, Bastero Acha I, Halder R, Cialini C, et al. Fiber deprivation and microbiome-borne curli shift gut bacterial populations and accelerate disease in a mouse model of Parkinson's disease. *Cell Rep*. 2023;42:113071.
- Huang B, Chau SWH, Liu Y, Chan JWY, Wang J, Ma SL, Zhang J, Chan PKS, Yeoh YK, Chen Z, et al. Gut microbiome dysbiosis across early Parkinson's disease, REM sleep behavior disorder and their first-degree relatives. *Nat Commun*. 2023;14:2501.
- Heintz-Buschart A, Pandey U, Wicke T, Sixel-Doring F, Janzen A, Sittig-Wiegand E, Trenkwalder C, Oertel WH, Mollenhauer B, Wilmes P. The nasal and gut microbiome in Parkinson's disease and idiopathic rapid eye movement sleep behavior disorder. *Mov Disord*. 2018;33:88–98.
- Zhang P, Huang P, Li Y, Du J, Luo N, He Y, Liu J, He G, Cui S, Zhang W, et al. Relationships between rapid eye movement sleep behavior disorder and Parkinson's disease: indication from gut microbiota alterations. *Aging Dis*. 2024;15:357–68.
- Hughes AJ, Daniel SE, Kilford L, Lees AJ. Accuracy of clinical diagnosis of idiopathic Parkinson's disease: a clinico-pathological study of 100 cases. *J Neurol Neurosurg Psychiatry*. 1992;55:181–4.
- Jo S, Kang W, Hwang YS, Lee SH, Park KW, Kim MS, Lee H, Yoon HJ, Park YK, Chalita M, et al. Oral and gut dysbiosis leads to functional alterations in Parkinson's disease. *NPJ Parkinsons Dis*. 2022;8:87.
- Na YJ, Lee SH. Development and validation of a quantitative food frequency questionnaire to assess nutritional status in Korean adults. *Nutr Res Pract*. 2012;6:444–50.
- Guidelines-Rome III Diagnostic criteria for functional gastrointestinal disorders. *J Gastrointest Liver Dis*. 2006;15:307–12.
- Postuma RB, Arnulf I, Hogl B, Iranzo A, Miyamoto T, Dauvilliers Y, Oertel W, Ju YE, Puligheddu M, Jennum P, et al. A single-question screen for rapid eye movement sleep behavior disorder: a multicenter validation study. *Mov Disord*. 2012;27:913–6.
- Martin M. Cutadapt removes adapter sequences from high-throughput sequencing reads. 2011;2011(17):3.
- Bolyen E, Rideout JR, Dillon MR, Bokulich NA, Abnet CC, Al-Ghalith GA, Alexander H, Alm EJ, Arumugam M, Asnicar F, et al. Reproducible, interactive, scalable and extensible microbiome data science using QIIME 2. *Nat Biotechnol*. 2019;37:852–7.
- Callahan BJ, McMurdie PJ, Rosen MJ, Han AW, Johnson AJ, Holmes SP. DADA2: high-resolution sample inference from Illumina amplicon data. *Nat Methods*. 2016;13:581–3.
- Pedregosa F, Varoquaux G, Gramfort A, Michel V, Thirion B, Grisel O, Blondel M, Prettenhofer P, Weiss R, Dubourg V, et al. Scikit-learn: machine learning in python. *J Mach Learn Res*. 2011;12:2825–30.
- Bokulich NA, Kaehler BD, Rideout JR, Dillon M, Bolyen E, Knight R, Huttenhower GA, Gregory Caporaso J. Optimizing taxonomic classification of marker-gene amplicon sequences with QIIME 2's q2-feature-classifier plugin. *Microbiome*. 2018;6:90.
- Quast C, Pruesse E, Yilmaz P, Gerken J, Schaefer T, Yarza P, Peplies J, Glockner FO. The SILVA ribosomal RNA gene database project: improved data processing and web-based tools. *Nucleic Acids Res*. 2013;41:D590–596.
- Robeson MS 2nd, O'Rourke DR, Kaehler BD, Ziemski M, Dillon MR, Foster JT, Bokulich NA. RESCRIPt: Reproducible sequence taxonomy reference database management. *PLoS Comput Biol*. 2021;17:e1009581.
- Mirarab S, Nguyen N, Warnow T. SEPP: SATE-enabled phylogenetic placement. In: *Biocomputing 2012*; 2012. p. 247–258.
- Janssen S, McDonald D, Gonzalez A, Navas-Molina JA, Jiang L, Xu ZZ, Winker K, Kado DM, Orwoll E, Manary M, et al. Phylogenetic placement of exact amplicon sequences improves associations with clinical information. *Msystems*. 2018;3(3):10–128.
- Mclver LJ, Abu-Ali G, Franzosa EA, Schwager R, Morgan XC, Waldron L, Segata N, Huttenhower C. bioBakery: a meta-omic analysis environment. *Bioinformatics*. 2018;34:1235–7.

31. Bolger AM, Lohse M, Usadel B. Trimmomatic: a flexible trimmer for Illumina sequence data. *Bioinformatics*. 2014;30:2114–20.
32. Langmead B, Salzberg SL. Fast gapped-read alignment with Bowtie 2. *Nat Methods*. 2012;9:357–9.
33. Blanco-Miguez A, Beghini F, Cumbo F, Mclver LJ, Thompson KN, Zolfo M, Manghi P, Dubois L, Huang KD, Thomas AM, et al. Extending and improving metagenomic taxonomic profiling with uncharacterized species using MetaPhlan 4. *Nat Biotechnol*. 2023;41:1633–44.
34. Beghini F, Mclver LJ, Blanco-Miguez A, Dubois L, Asnicar F, Maharjan S, Mailyan A, Manghi P, Scholz M, Thomas AM, et al. Integrating taxonomic, functional, and strain-level profiling of diverse microbial communities with bioBakery 3. *Elife*. 2021;10:e65088.
35. Suzek BE, Wang Y, Huang H, McGarvey PB, Wu CH, UniProt C. UniRef clusters: a comprehensive and scalable alternative for improving sequence similarity searches. *Bioinformatics*. 2015;31:926–32.
36. Kanehisa M, Goto S. KEGG: kyoto encyclopedia of genes and genomes. *Nucleic Acids Res*. 2000;28:27–30.
37. Kanehisa M, Sato Y. KEGG Mapper for inferring cellular functions from protein sequences. *Protein Sci*. 2020;29:28–35.
38. Luo W, Brouwer C. Pathview: an R/Bioconductor package for pathway-based data integration and visualization. *Bioinformatics*. 2013;29:1830–1.
39. Wu T, Hu E, Xu S, Chen M, Guo P, Dai Z, Feng T, Zhou L, Tang W, Zhan L, et al. clusterProfiler 4.0: a universal enrichment tool for interpreting omics data. *Innovation (Camb)*. 2021;2:100141.
40. Wallen ZD, Demirkan A, Twa G, Cohen G, Dean MN, Standaert DG, Sampson TR, Payami H. Metagenomics of Parkinson's disease implicates the gut microbiome in multiple disease mechanisms. *Nat Commun*. 2022;13:6958.
41. Lozupone C, Knight R. UniFrac: a new phylogenetic method for comparing microbial communities. *Appl Environ Microbiol*. 2005;71:8228–35.
42. Mallick H, Rahnavard A, Mclver LJ, Ma S, Zhang Y, Nguyen LH, Tickle TL, Weingart G, Ren B, Schwager EH, et al. Multivariable association discovery in population-scale meta-omics studies. *PLoS Comput Biol*. 2021;17:e1009442.
43. Lin H, Peddada SD. Analysis of compositions of microbiomes with bias correction. *Nat Commun*. 2020;11:3514.
44. Frioux C, Ansoorge R, Ozkurt E, Ghassemi Nedjad C, Fritscher J, Quince C, Waszak SM, Hildebrand F. Enterosignatures define common bacterial guilds in the human gut microbiome. *Cell Host Microbe*. 2023;31:1111–1125 e1116.
45. Danecek P, Bonfield JK, Liddle J, Marshall J, Ohan V, Pollard MO, Whitwham A, Keane T, McCarthy SA, Davies RM, Li H. Twelve years of SAMtools and BCFtools. *Gigascience*. 2021;10:giab008.
46. Nurk S, Meleshko D, Korobeynikov A, Pevzner PA. metaSPAdes: a new versatile metagenomic assembler. *Genome Res*. 2017;27:824–34.
47. Kang DD, Li F, Kirton E, Thomas A, Egan R, An H, Wang Z. MetaBAT 2: an adaptive binning algorithm for robust and efficient genome reconstruction from metagenome assemblies. *PeerJ*. 2019;7:e7359.
48. Wu YW, Simmons BA, Singer SW. MaxBin 2.0: an automated binning algorithm to recover genomes from multiple metagenomic datasets. *Bioinformatics*. 2016;32:605–7.
49. Alneberg J, Bjarnason BS, de Bruijn I, Schirmer M, Quick J, Ijaz UZ, Lahti L, Loman NJ, Andersson AF, Quince C. Binning metagenomic contigs by coverage and composition. *Nat Methods*. 2014;11:1144–6.
50. Sieber CMK, Probst AJ, Sharrar A, Thomas BC, Hess M, Tringe SG, Banfield JF. Recovery of genomes from metagenomes via a dereplication, aggregation and scoring strategy. *Nat Microbiol*. 2018;3:836–43.
51. Parks DH, Imelfort M, Skennerton CT, Hugenholtz P, Tyson GW. CheckM: assessing the quality of microbial genomes recovered from isolates, single cells, and metagenomes. *Genome Res*. 2015;25:1043–55.
52. Chaumeil PA, Mussig AJ, Hugenholtz P, Parks DH. GTDB-Tk: a toolkit to classify genomes with the genome taxonomy database. *Bioinformatics*. 2019;36:1925–7.
53. Hyatt D, Chen GL, Locascio PF, Land ML, Larimer FW, Hauser LJ. Prodigal: prokaryotic gene recognition and translation initiation site identification. *BMC Bioinformatics*. 2010;11:119.
54. Seemann T. Prokka: rapid prokaryotic genome annotation. *Bioinformatics*. 2014;30:2068–9.
55. Aramaki T, Blanc-Mathieu R, Endo H, Ohkubo K, Kanehisa M, Goto S, Ogata H. KofamKOALA: KEGG Ortholog assignment based on profile HMM and adaptive score threshold. *Bioinformatics*. 2020;36:2251–2.
56. Sievers F, Higgins DG. Clustal omega for making accurate alignments of many protein sequences. *Protein Sci*. 2018;27:135–45.
57. Nguyen LT, Schmidt HA, von Haeseler A, Minh BQ. IQ-TREE: a fast and effective stochastic algorithm for estimating maximum-likelihood phylogenies. *Mol Biol Evol*. 2015;32:268–74.
58. Zheng J, Ge Q, Yan Y, Zhang X, Huang L, Yin Y. dbCAN3: automated carbohydrate-active enzyme and substrate annotation. *Nucleic Acids Res*. 2023;51:W115–21.
59. Liao Y, Smyth GK, Shi W. featureCounts: an efficient general purpose program for assigning sequence reads to genomic features. *Bioinformatics*. 2014;30:923–30.
60. Shannon P, Markiel A, Ozier O, Baliga NS, Wang JT, Ramage D, Amin N, Schwikowski B, Ideker T. Cytoscape: a software environment for integrated models of biomolecular interaction networks. *Genome Res*. 2003;13:2498–504.
61. Kelly BJ, Gross R, Bittiger K, Sherrill-Mix S, Lewis JD, Collman RG, Bushman FD, Li H. Power and sample-size estimation for microbiome studies using pairwise distances and PERMANOVA. *Bioinformatics*. 2015;31:2461–8.
62. Palacios N, Wilkinson J, Bjornevik K, Schwarzschild MA, Mclver L, Ascherio A, Huttenhower C. Metagenomics of the gut microbiome in Parkinson's disease: prodromal changes. *Ann Neurol*. 2023;94:486–501.
63. Bedarf JR, Hildebrand F, Coelho LP, Sunagawa S, Bahram M, Goeser F, Bork P, Wüllner U. Functional implications of microbial and viral gut metagenome changes in early stage L-DOPA-naïve Parkinson's disease patients. *Genome Med*. 2017;9:39.
64. Keshavarzian A, Green SJ, Engen PA, Voigt RM, Naqib A, Forsyth CB, Mutlu E, Shannon KM. Colonic bacterial composition in Parkinson's disease. *Mov Disord*. 2015;30:1351–60.
65. Hill-Burns EM, Debelius JW, Morton JT, Wissemann WT, Lewis MR, Wallen ZD, Peddada SD, Factor SA, Molho E, Zabetian CP, et al. Parkinson's disease and Parkinson's disease medications have distinct signatures of the gut microbiome. *Mov Disord*. 2017;32:739–49.
66. Li Z, Liang H, Hu Y, Lu L, Zheng C, Fan Y, Wu B, Zou T, Luo X, Zhang X, et al. Gut bacterial profiles in Parkinson's disease: a systematic review. *CNS Neurosci Ther*. 2023;29:140–57.
67. Fang P, Kazmi SA, Jameson KG, Hsiao EY. The Microbiome as a Modifier of Neurodegenerative Disease Risk. *Cell Host Microbe*. 2020;28:201–22.
68. Wang C, Lau CY, Ma F, Zheng C. Genome-wide screen identifies curli amyloid fibril as a bacterial component promoting host neurodegeneration. *Proc Natl Acad Sci*. 2021;118(34):e2106504118.
69. Bhoite SS, Han Y, Ruotolo BT, Chapman MR. Mechanistic insights into accelerated alpha-synuclein aggregation mediated by human microbiome-associated functional amyloids. *J Biol Chem*. 2022;298:102088.
70. Miller AL, Bessho S, Grando K, Tukul C. Microbiome or infections: amyloid-containing biofilms as a trigger for complex human diseases. *Front Immunol*. 2021;12:638867.
71. Berkhout MD, Plugge CM, Belzer C. How microbial glycosyl hydrolase activity in the gut mucosa initiates microbial cross-feeding. *Glycobiology*. 2022;32:182–200.
72. Boktor JC, Sharon G, Verhagen Metman LA, Hall DA, Engen PA, Zreloff Z, Hakim DJ, Bostick JW, Ousey J, Lange D, et al. Integrated multi-cohort analysis of the Parkinson's disease gut metagenome. *Mov Disord*. 2023;38:399–409.
73. Nishiwaki H, Ito M, Ishida T, Hamaguchi T, Maeda T, Kashiwara K, Tsuboi Y, Ueyama J, Shimamura T, Mori H, et al. Meta-analysis of gut dysbiosis in Parkinson's disease. *Mov Disord*. 2020;35:1626–35.
74. Zhou X, Baumann R, Gao X, Mendoza M, Singh S, Sand IK, et al. Gut microbiome of multiple sclerosis patients and paired household healthy controls reveal associations with disease risk and course. *Cell*. 2022;185:3467–3486.e3416.
75. Deehan EC, Duar RM, Armet AM, Perez-Muñoz ME, Jin M, Walter J. Modulation of the gastrointestinal microbiome with nondigestible fermentable carbohydrates to improve human health. *Microbiol Spectr*. 2017;5(5):10–128.
76. Kovatcheva-Datchary P, Nilsson A, Akrami R, Lee YS, De Vadder F, Arora T, Hallen A, Martens E, Bjorck I, Backhed F. Dietary fiber-induced

- improvement in glucose metabolism is associated with increased abundance of *Prevotella*. *Cell Metab.* 2015;22:971–82.
77. Chen R, Zhang C, Xu F, Yu L, Tian F, Chen W, Zhai Q. Meta-analysis reveals gut microbiome and functional pathway alterations in response to resistant starch. *Food Funct.* 2023;14:5251–63.
 78. Lee DW, Ryu YK, Chang DH, Park HY, Go J, Maeng SY, Hwang DY, Kim BC, Lee CH, Kim KS. *Agathobaculum butyriciproducens* shows neuro-protective effects in a 6-OHDA-induced mouse model of Parkinson's disease. *J Microbiol Biotechnol.* 2022;32:1168–77.
 79. Duan M, Liu F, Fu H, Lu S, Wang T. Preoperative microbiomes and intestinal barrier function can differentiate prodromal Alzheimer's disease from normal neurocognition in elderly patients scheduled to undergo orthopedic surgery. *Front Cell Infect Microbiol.* 2021;11:592842.
 80. Wang G, Zou D, Lu X, Gu X, Cheng Y, Qi T, Cheng Y, Yu J, Ye M, Zhou P. Gut microbiota alteration in disease progression of neurosyphilis. *Infect Drug Resist.* 2022;15:6603–12.
 81. Liu S, Li E, Sun Z, Fu D, Duan G, Jiang M, Yu Y, Mei L, Yang P, Tang Y, Zheng P. Altered gut microbiota and short chain fatty acids in Chinese children with autism spectrum disorder. *Sci Rep.* 2019;9:287.
 82. Jiang L, Li JC, Tang BS, Guo JF. Associations between gut microbiota and Parkinson disease: a bidirectional Mendelian randomization analysis. *Eur J Neurol.* 2023;30:3471–7.
 83. Shin NR, Whon TW, Bae JW. Proteobacteria: microbial signature of dysbiosis in gut microbiota. *Trends Biotechnol.* 2015;33:496–503.
 84. Zeng MY, Inohara N, Nunez G. Mechanisms of inflammation-driven bacterial dysbiosis in the gut. *Mucosal Immunol.* 2017;10:18–26.
 85. Thongsomboon W, Serra DO, Possling A, Hadjineophytou C, Hengge R, Cegelski L. Phosphoethanolamine cellulose: a naturally produced chemically modified cellulose. *Science.* 2018;359:334–8.
 86. Hollenbeck EC, Antonoplis A, Chai C, Thongsomboon W, Fuller GG, Cegelski L. Phosphoethanolamine cellulose enhances curli-mediated adhesion of uropathogenic *Escherichia coli* to bladder epithelial cells. *Proc Natl Acad Sci U S A.* 2018;115:10106–11.
 87. Serra DO, Hengge R. Bacterial multicellularity: the biology of *Escherichia coli* building large-scale biofilm communities. *Annu Rev Microbiol.* 2021;75:269–90.
 88. Wang X, Chapman MR. Sequence determinants of bacterial amyloid formation. *J Mol Biol.* 2008;380:570–80.
 89. Wang X, Zhou Y, Ren JJ, Hammer ND, Chapman MR. Gatekeeper residues in the major curlin subunit modulate bacterial amyloid fiber biogenesis. *Proc Natl Acad Sci U S A.* 2010;107:163–8.
 90. Park JT, Uehara T. How bacteria consume their own exoskeletons (turnover and recycling of cell wall peptidoglycan). *Microbiol Mol Biol Rev.* 2008;72:211–27, table of contents.
 91. Konopka JB. N-acetylglucosamine (GlcNAc) functions in cell signaling. *Scientifica (Cairo)* 2012;2012:489208.
 92. Barnhart MM, Lynem J, Chapman MR. GlcNAc-6P levels modulate the expression of Curli fibers by *Escherichia coli*. *J Bacteriol.* 2006;188:5212–9.
 93. Wardman JF, Bains RK, Rahfeld P, Withers SG. Carbohydrate-active enzymes (CAZymes) in the gut microbiome. *Nat Rev Microbiol.* 2022;20:542–56.
 94. Desai MS, Seekatz AM, Koropatkin NM, Kamada N, Hickey CA, Wolter M, Pudlo NA, Kitamoto S, Terrapon N, Muller A, et al. A dietary fiber-deprived gut microbiota degrades the colonic mucus barrier and enhances pathogen susceptibility. *Cell.* 2016;167(1339–1353):e1321.
 95. Neumann M, Steimle A, Grant ET, Wolter M, Parrish A, Willieme S, Brenner D, Martens EC, Desai MS. Deprivation of dietary fiber in specific-pathogen-free mice promotes susceptibility to the intestinal mucosal pathogen *Citrobacter rodentium*. *Gut Microbes.* 2021;13:1966263.
 96. Yamaguchi M, Yamamoto K. Mucin glycans and their degradation by gut microbiota. *Glycoconj J.* 2023;40:493–512.
 97. Makki K, Deehan EC, Walter J, Backhed F. The impact of dietary fiber on gut microbiota in host health and disease. *Cell Host Microbe.* 2018;23:705–15.
 98. Ranaivo H, Thirion F, Bera-Maillet C, Guilly S, Simon C, Sothier M, Van Den Berghe L, Feugier-Favier N, Lambert-Porcheron S, Dussous I, et al. Increasing the diversity of dietary fibers in a daily-consumed bread modifies gut microbiota and metabolic profile in subjects at cardio-metabolic risk. *Gut Microbes.* 2022;14:2044722.
 99. Rosario D, Bidkhorji G, Lee S, Bedarf J, Hildebrand F, Le Chatelier E, Uhlen M, Ehrlich SD, Proctor G, Wüllner U, et al. Systematic analysis of gut microbiome reveals the role of bacterial folate and homocysteine metabolism in Parkinson's disease. *Cell Rep.* 2021;34:108807.
 100. Barnhart MM, Chapman MR. Curli biogenesis and function. *Annu Rev Microbiol.* 2006;60:131–47.
 101. Rawat PS, Li Y, Zhang W, Meng X, Liu W. *Hungatella hathewayi*, an efficient glycosaminoglycan-degrading firmicutes from human gut and its chondroitin ABC exolyase with high activity and broad substrate specificity. *Appl Environ Microbiol.* 2022;88:e0154622.
 102. Parrish A, Boudaud M, Grant ET, Willieme S, Neumann M, Wolter M, Craig SZ, De Sciscio A, Cosma A, Hunewald O, et al. *Akkermansia muciniphila* exacerbates food allergy in fibre-deprived mice. *Nat Microbiol.* 2023;8:1863–79.
 103. Houser MC, Chang J, Factor SA, Molho ES, Zabetian CP, Hill-Burns EM, Payami H, Hertzberg VS, Tansey MG. Stool immune profiles evince gastrointestinal inflammation in Parkinson's disease. *Mov Disord.* 2018;33:793–804.
 104. Matheoud D, Cannon T, Voisin A, Penttinen AM, Ramet L, Fahmy AM, Ducrot C, Laplante A, Bourque MJ, Zhu L, et al. Intestinal infection triggers Parkinson's disease-like symptoms in *Pink1(-/-)* mice. *Nature.* 2019;571:565–9.
 105. Perez-Pardo P, Dodiya HB, Engen PA, Forsyth CB, Huschens AM, Shaikh M, Voigt RM, Naqib A, Green SJ, Kordower JH, et al. Role of TLR4 in the gut-brain axis in Parkinson's disease: a translational study from men to mice. *Gut.* 2019;68:829–43.
 106. Nerius M, Doblhammer G, Tamguney G. GI infections are associated with an increased risk of Parkinson's disease. *Gut.* 2020;69:1154–6.
 107. Lee HS, Lobbstaal E, Vermeire S, Sabino J, Cleynen I. Inflammatory bowel disease and Parkinson's disease: common pathophysiological links. *Gut.* 2021;70:408–17.
 108. Reynolds A, Mann J, Cummings J, Winter N, Mete E, Te Morenga L. Carbohydrate quality and human health: a series of systematic reviews and meta-analyses. *Lancet.* 2019;393:434–45.
 109. Levy M, Kolodziejczyk AA, Thaiss CA, Elinav E. Dysbiosis and the immune system. *Nat Rev Immunol.* 2017;17:219–32.
 110. Forsyth CB, Shannon KM, Kordower JH, Voigt RM, Shaikh M, Jaglin JA, Estes JD, Dodiya HB, Keshavarzian A. Increased intestinal permeability correlates with sigmoid mucosa alpha-synuclein staining and endotoxin exposure markers in early Parkinson's disease. *PLoS ONE.* 2011;6:e28032.
 111. Kelly LP, Carvey PM, Keshavarzian A, Shannon KM, Shaikh M, Bakay RA, Kordower JH. Progression of intestinal permeability changes and alpha-synuclein expression in a mouse model of Parkinson's disease. *Mov Disord.* 2014;29:999–1009.
 112. Clairembault T, Leclair-Visonneau L, Coron E, Bourreille A, Le Dily S, Vavasseur F, Heymann MF, Neunlist M, Derkinderen P. Structural alterations of the intestinal epithelial barrier in Parkinson's disease. *Acta Neuropathol Commun.* 2015;3:12.
 113. Levine PM, Galesic A, Balana AT, Mahul-Mellier AL, Navarro MX, De Leon CA, Lashuel HA, Pratt MR. α -Synuclein O-GlcNAcylation alters aggregation and toxicity, revealing certain residues as potential inhibitors of Parkinson's disease. *Proc Natl Acad Sci U S A.* 2019;116:1511–9.
 114. Lee BE, Kim HY, Kim HJ, Jeong H, Kim BG, Lee HE, Lee J, Kim HB, Lee SE, Yang YR, et al. O-GlcNAcylation regulates dopamine neuron function, survival and degeneration in Parkinson disease. *Brain.* 2020;143:3699–716.
 115. Naseem S, Konopka JB. N-acetylglucosamine regulates virulence properties in microbial pathogens. *PLoS Pathog.* 2015;11:e1004947.
 116. Hesketh GG, Dennis JW. N-acetylglucosamine: more than a silent partner in insulin resistance. *Glycobiology.* 2017;27:595–8.

Publisher's Note

Springer Nature remains neutral with regard to jurisdictional claims in published maps and institutional affiliations.